Manuscript prepared for Geosci. Model Dev.
with version 2014/07/29 7.12 Copernicus papers of the LaTeX class copernicus.cls.
Date: 29 August 2016

Ozone air quality simulations with WRF-Chem (v3.5.1) over Europe: Model evaluation and chemical mechanism comparison

Kathleen A. Mar[1], Narendra Ojha[2], Andrea Pozzer[2], and Tim M. Butler[1]

[1]Institute for Advanced Sustainability Studies, Potsdam, Germany
[2]Atmospheric Chemistry Department, Max Planck Institute for Chemistry, Mainz, Germany

Correspondence to: K. A. Mar (Kathleen.Mar@iass-potsdam.de)

1 **Abstract.** We present an evaluation of the online regional model WRF-Chem over Europe with a fo-
2 cus on ground-level ozone (O_3) and nitrogen oxides (NO_x). The model performance is evaluated for
3 two chemical mechanisms, MOZART- 4 and RADM2, for year-long simulations. Model-predicted
4 surface meteorological variables (e.g., temperature, wind speed and direction) compared well overall
5 with surface-based observations, consistent with other WRF studies. WRF-Chem simulations em-
6 ploying MOZART- 4 as well as RADM2 chemistry were found to reproduce the observed spatial
7 variability in surface ozone over Europe. However, the absolute O_3 concentrations predicted by the
8 two chemical mechanisms were found to be quite different, with MOZART- 4 predicting O_3 concen-
9 trations up to $20\,\mu g\,m^{-3}$ greater than RADM2 in summer. Compared to observations, MOZART- 4
10 chemistry overpredicted O_3 concentrations for most of Europe in the summer and fall, with a sum-
11 mertime domain-wide mean bias of $+10\,\mu g\,m^{-3}$ against observations from the AirBase network. In
12 contrast, RADM2 chemistry generally led to an underestimation of O_3 over the European domain in
13 all seasons. We found that the use of the MOZART- 4 mechanism, evaluated here for the first time
14 for a European domain, led to lower absolute biases than RADM2 when compared to ground-based
15 observations. The two mechanisms show relatively similar behavior for NO_x, with both MOZART- 4
16 and RADM2 resulting in a slight underestimation of NO_x compared to surface observations. Further
17 investigation into the differences between the two mechanisms revealed that the net midday photo-
18 chemical production rate of O_3 in summer is higher for MOZART- 4 than for RADM2 for most
19 of the domain. The largest differences in O_3 production can be seen over Germany, where net O_3
20 production in MOZART- 4 is seen to be higher than in RADM2 by $1.8\,ppb\,hr^{-1}$ ($3.6\,\mu g\,m^{-3}\,hr^{-1}$)
21 or more. We also show that, while the two mechanisms exhibit similar NO_x-sensitivity, RADM2 is
22 approximately twice as sensitive to increases in anthropogenic VOC emissions as MOZART- 4. Ad-

ditionally, we found that differences in reaction rate coefficients for inorganic gas phase chemistry in MOZART- 4 vs. RADM2 accounted for a difference of 8 $\mu g\,m^{-3}$, or 40% of the summertime difference in O_3 predicted by the two mechanisms. Differences in deposition and photolysis schemes explained smaller differences in O_3. Our results highlight the strong dependence of modeled surface O_3 over Europe on the choice of gas phase chemical mechanism, which we discuss in the context of overall uncertainties in prediction of ground-level O_3 and its associated health impacts (via the health-related metrics MDA8 and SOMO35).

1 Introduction

Tropospheric ozone (O_3) is an air pollutant with adverse effects on human and ecosystem health as well as a short-lived climate forcer with a significant warming effect (e.g., Monks et al., 2015; Stevenson et al., 2013; WHO, 2003). In Europe, ozone pollution remains a problem: the European Environmental Agency reports that between 2010 and 2012, 98% of Europe's urban population was exposed to O_3 levels in exceedance of the WHO air quality guideline (EEA, 2014), leading to more than 6000 premature deaths annually (Lelieveld et al., 2015). This is despite the fact that European emissions of ozone precursors, in particular nitrogen oxides (NO_x) and volatile organic compounds (VOCs), have decreased significantly since 1990. The persistance of unhealthy levels of ozone in Europe can be attributed to increases in hemispheric background ozone (Wilson et al., 2012) as well as the non-linear relationship between O_3 and levels of precursor species NO_x and VOC (EEA, 2014).

Air quality models are employed to understand the drivers of air pollution at a regional scale and to evaluate the roles of and interactions between emissions, meteorology and chemistry. These models fall into two broad categories: offline Chemistry-Transport Models (CTMs), in which meteorology is calculated separately from model chemistry, and "online" models, the category to which WRF-Chem belongs, in which the meteorology and chemistry are coupled, meaning they are solved together in a physically consistent manner (e.g., Zhang, 2008). The meteorology and chemistry components in WRF-Chem use the same horizontal and vertical grids and same timestep, eliminating the need for temporal interpolation (e.g., Grell et al., 2004, 2005).

Air quality modeling studies over the European region have predominantly utilized CTMs, examples of which include EMEP (Simpson et al., 2012), CHIMERE (Terrenoire et al., 2015), and LOTOS-EUROS (Schaap et al., 2008). The application of online coupled regional meteorology-chemistry models in Europe, among them WRF-Chem, has been recently reviewed by Baklanov et al. (2014). The use of WRF-Chem over Europe has increased in recent years (e.g., Forkel et al., 2012; Žabkar et al., 2015; Solazzo et al., 2012a, b; Tuccella et al., 2012; Zhang et al., 2013a, b). However, only a limited number of these studies are dedicated to the evaluation of WRF-Chem-simulated meteorology and chemistry over the whole European domain. The study of Tuccella et al. (2012) evaluated the performance of WRF-Chem using the RADM2 chemical mechanism by comparing domain-wide average values against observations of meteorology and chemistry. However, an evaluation of the spatial distribution of model-simulated meteorology and trace gases is missing. This type of spatial information is extremely pertinent for air quality management applications, where model performance at a national scale can become more relevant than performance metrics applied to the whole of Europe; this information gets lost when only comparing quantities that have been averaged over the entire domain. Additionally, Tuccella et al. (2012) utilized time-invariant chemical boundary conditions, which the authors suggested misrepresented the seasonal changes in the intercontinental transport (Tuccella et al., 2012). The importance of temporally varying chemical

67 boundary conditions in air quality modeling has also been stressed in other studies (including Akri-
68 tidis et al., 2013; Andersson et al., 2015). In addition to the study of Tuccella et al. (2012), Zhang
69 et al. (2013b) evaluated the performance WRF-Chem-MADRID (Zhang et al., 2010), an unofficial
70 version of WRF-Chem coupled to the Model of Aerosol Dynamics, Reaction, Ionization, and Dis-
71 solution (MADRID), over Europe for the month of July 2001, employing the gas-phase mechanism
72 CB05 (Yarwood et al., 2005). This detailed study provides a valuable reference for comparison to
73 the present work, but their simulations are only for one month, rather than the complete seasonal
74 cycle.

75   Several groups contributed WRF-Chem simulations to the AQMEII project (phase 1 and phase 2)
76 for the European domain (Solazzo et al., 2012b; Im et al., 2015). In AQMEII phase 1, two differ-
77 ent WRF-Chem simulations were part of the model ensemble for Europe, but evaluation of model
78 performance for ozone focused on evaluation of the ensemble (Solazzo et al., 2012b), rather than
79 on individual members. In fact, in the analysis of Solazzo et al. (2012b), individual models were
80 anonymized, meaning the performance statistics for the WRF-Chem ensemble members are not ex-
81 plicitly presented. The evaluation of model performance with respect to ozone in AQMEII phase 2
82 (Im et al., 2015) provides more information on the model performance of the contributing WRF-
83 Chem ensemble members for the European domain. In AQMEII phase 2, seven different WRF-Chem
84 runs were part of the ensemble. Of these seven simulations, four of them used the gas phase chemical
85 mechanism RADM2 (Stockwell et al., 1990), two used the mechanism CBMZ (Zaveri and Peters,
86 1999), and one used the mechanism RACM (Stockwell et al., 1997; Geiger et al., 2003). All WRF-
87 Chem simulations for Europe in AQMEII phase 2 tended to underestimate ozone concentrations,
88 with annual average normalized mean bias ranging from -1.6 to -15.8 %, depending on the ensemble
89 member.

90   The purpose of the present study is to perform a detailed evaluation of meteorology and gas phase
91 chemistry simulated by WRF-Chem, including the spatial and seasonal variations over a full year
92 seasonal cycle using time-varying chemical boundary conditions. This evaluation is performed for
93 two different gas phase chemical mechanisms within WRF-Chem, MOZART- 4 (Emmons et al.,
94 2010) and RADM2 (Stockwell et al., 1990). As discussed above, the RADM2 mechanism has been
95 popularly used in WRF-Chem for simulation over Europe (Tuccella et al., 2012; Im et al., 2015). The
96 MOZART- 4 chemical mechanism has been widely used with WRF-Chem for regional air quality
97 applications outside of Europe (e.g., Pfister et al., 2013; Im et al., 2015). To the authors' knowledge,
98 however, WRF-Chem with MOZART- 4 has not yet been applied and evaluated over a European
99 domain.

100   The simultaneous evaluation of WRF-Chem with two different chemical mechanisms further al-
101 lows us to evaluate the sensitivity of O_3 and NO_x to the choice of chemical mechanism in a setup
102 where the differences in model physics and other parameters are minimized. This is in contrast to
103 the study of Im et al. (2015), where the various WRF-Chem ensemble members also used different

schemes for model physics. Coates and Butler (2015) recently investigated the sensitivity of the production of odd oxygen (O_x, a proxy for production of O_3) to the choice of chemical mechanism using a box model, and found that choice of chemical mechanism led to differences in O_3 concentrations on the order of 10 ppb under idealized conditions, although differences between the MOZART- 4 and RADM2 chemical mechanisms tended to be closer to 5 ppb. In another box model study, Knote et al. (2015) investigated the sensitivity of O_3, NO_x, and other radicals to the different gas-phase chemical mechanisms used in the models that contributed to the AQMEII phase-2 intercomparison project. Knote et al. (2015) found that the choice of chemical mechanism is responsible for a 5% uncertainty in predicted O_3 concentrations and a 25% uncertainty in predicted NO_x concentrations.

The present study builds on the work of Coates and Butler (2015) and Knote et al. (2015) by comparing two chemical mechanisms within an online coupled regional air quality model. The use of WRF-Chem provides an advantage in that it is compatible with multiple different chemical mechanisms, allowing us to test the effect of different chemistry with minimal confounding factors due to differences in model physics, etc. Furthermore, the use of an online regional model rather than a box model allows us to examine the sensitivity of model-predicted concentrations to the choice of chemical mechanism under more realistic conditions, in which variations in meteorology and dynamics are fully included. Parameters such as radiation are allowed to vary realistically, and different chemical regimes (NO_x- vs. VOC-limited) are present (e.g., in different seasons and in different parts of the model domain).

Chemical mechanism comparisons have also been undertaken previously using 3-D regional air quality models, though the majority have focused on comparing the SAPRC-99 mechanism (Carter, 1990) with versions of the Carbon Bond mechanism (Gery et al., 1989) over a U.S. domain (Luecken et al., 2008; Faraji et al., 2008; Yarwood et al., 2003; Zhang et al., 2012). Two additional studies have compared versions of the RACM mechanism with RADM2 (Mallet and Sportisse, 2006) and CB05 (Kim et al., 2010) using the model Polyphemus (Mallet et al., 2007) for a European domain. Typically, these studies found that simulations using two different chemical mechanisms led to differences in O_3 on the order of 5-10 ppb (Luecken et al., 2008; Zhang et al., 2012; Mallet and Sportisse, 2006; Kim et al., 2010), although extreme differences of 30-40 ppb were observed between SAPRC-99 and CB-IV mechanisms when simulating high ozone episodes (Faraji et al., 2008; Yarwood et al., 2003).

In this paper, the model configuration, including emissions and initial and boundary conditions, is described in Section 2. A description of observational datasets for meteorology and chemistry and the evaluation methodology is provided in Section 3. Results for the model evaluation and intercomparison of two chemical are presented in Section 4 followed by a summary and concluding remarks in Section 5.

2 Model Description and Setup

2.1 WRF-Chem

This study utilizes the Weather Research and Forecasting with Chemistry (WRF-Chem) model (http://ruc.noaa.gov/wrf/WG11) version 3.5.1. WRF-Chem has been developed collaboratively by NOAA, DOE/PNNL, NCAR and other research institutes (https://www2.acd.ucar.edu/wrf-chem).

We defined our simulation domain on the Lambert projection. The model domain is centered at $15°$ E, $52°$ N, and covers nearly the entire European region. The horizontal resolution is chosen to be $45\,km \times 45\,km$. The model domain has 115 and 100 grid points in the west-east and south-north directions respectively.

We have used 35 vertical levels in the model starting from surface to $10\,hPa$. The lowest model level corresponds to an approximate altitude of $50\,m$ above the surface. Tests have shown that surface layer concentrations in this configuration are effectively the same as when the lowest model level is at a height of $14\,m$, but with no urban surface physics scheme (the urban physics scheme is incompatible with a 14-m model level). Geographical data including terrain height, soil properties, albedo, etc. are interpolated primarily from USGS (United States Geological Survey data (Wang et al., 2014)) at $30\,sec$ resolution. The land use classification has been interpolated from the CORINE data (EEA, 2012) at $250\,m$ resolution, which was then mapped to the USGS land use classes used by WRF (see Kuik et al., 2016).

Model simulations are conducted for the period of 23 December 2006 to 31 December 2007. The first week of output was treated as model spin up and has been discarded. The instantaneous model output, stored every hour, has been used for the analysis. The different options used in this study to parametrize the atmospheric processes are listed in Table 1. A namelist is available in the Supplementary Material.

The initial and lateral boundary conditions for the meteorological fields were provided from the ERA-interim reanalysis dataset available from ECMWF (http://www.ecmwf.int/en/research/climate-reanalysis/era-interim). This data is available every $6\,hours$ with a spatial resolution of approximately $80\,km$ (T255 spectral). In order to limit the errors in the WRF simulated meteorology the Four Dimensional Data Assimilation (FDDA) has been applied. In the FDDA, temperature is nudged at all the vertical levels with a nudging coefficient of 0.0003. The horizontal winds are nudged at all the vertical levels, except within the PBL, with the nudging coefficient of 0.0003. Sensitivity studies performed showed that nudging of water vapor highly suppressed the precipitation over Europe in a manner inconsistent with observations. As such, water vapor is not nudged in our simulations. This also follows the approach of, e.g., Miguez-Macho et al. (2004) and Stegehuis et al. (2014). The nudging coefficients for temperature and winds have been chosen following previous studies (Stauffer et al., 1991; Liu et al., 2012). The time step for the simulations has been set at $180\,s$.

174   Initial and boundary conditions for chemical fields in WRF-Chem are used from the MOZART-
175   4/GEOS5 simulations (http://www.acd.ucar.edu/wrf-chem/mozart.shtml), with a horizontal resolu-
176   tion of $1.9° \times 2.5°$ and 56 pressure levels. MOZART- 4/GEOS-5 simulations use meteorology from
177   the NASA GMAO GEOS-5 model and emissions based on ARCTAS inventory (http://www.cgrer.
178   uiowa.edu/arctas/emission.html).

179   2.2   Emissions

180   Anthropogenic emissions of CO, NO_x, SO_2, NMVOCs, PM_{10}, PM_{25}, and NH_3 are used from the
181   TNO-MACC II emission inventory for Europe (Kuenen et al., 2014), for the year 2007. These emis-
182   sions are provided as yearly totals by source sector on a high-resolution ($7\,km \times 7\,km$) grid. The
183   TNO-MACC II emission inventory is based on emissions reported by member countries to the Eu-
184   ropean Monitoring and Evaluation Program (EMEP), which are then further refined to fill gaps and
185   correct errors and obvious inconsistencies. Emissions are temporally disaggregated based on sea-
186   sonal, weekly and diurnal cycles provided by Denier van der Gon et al. (2011); Schaap et al. (2005).
187   These temporal profiles vary by source sector according to the SNAP (Selected Nomenclature for
188   Sources of Air Pollution) convention. NMVOC emissions are split into modeled NMVOC species
189   (e.g., ethane, aldehydes) based on von Schneidemesser et al. (2016). NO_x is emitted as 90% NO and
190   10% NO_2 by mole. Emissions are distributed into the first seven model vertical layers (the surface
191   and the first 6 model layers above the surface) based on sectoral averages from (Bieser et al., 2011),
192   although model runs showed little sensitivity to the distribution of emissions above the surface layer.
193   The model domain used in this study is larger than the European domain used in the TNO-
194   MACC II inventory (Kuenen et al., 2014). Emissions at our domain edges were filled using the
195   Hemispheric Transport of Air Pollution (HTAP v2.2) emission inventory for the year 2008 (http:
196   //edgar.jrc.ec.europa.eu/htap_v2/index.php). The HTAP v2 data, described in detail by Janssens-
197   Maenhout et al. (2015), is harmonized at a spatial resolution of $0.1° \times 0.1°$ and available with
198   monthly time resolution. In our model simulations, no additional weekly or diurnal profiles were
199   applied to the HTAP v2 emissions. Furthermore, all emissions from HTAP were emitted into the
200   surface model layer. Because HTAP emissions were only used at the grid "edge," the differences in
201   temporal and vertical resolution of emissions used for HTAP is not expected to have a significant
202   impact on model results. An example of emissions processed for model input is shown Figure S1 in
203   the Supplementary Material.
204   Biomass burning emissions are from the Fire Inventory from NCAR (FINN), Version 1 (Wiedin-
205   myer et al., 2011). To avoid the double counting of emissions from agricultural burning (i.e., assum-
206   ing that the FINN product captures large-scale agricultural burning), emissions of the combustion
207   species CO, NO_x, and SO_2 from SNAP category 10 (Agriculture) in the TNO-MACC II inventory
208   were not included in model simulations, at the suggestion of H.A.C. van der Gon (personal commu-

209   nication, 2015). Biogenic Emissions are calculated online based on weather and land use data using

210   the Model of Emissions of Gases and Aerosols from Nature (MEGAN) (Guenther et al., 2006).

211   **2.3   Model Chemistry**

212   The two year-long WRF-Chem simulations performed for this study are summarized in Table 2. In

213   the MOZART simulation, gas phase chemistry is represented by the Model for Ozone and Related

214   chemical Tracers, version 4 (MOZART- 4) mechanism (Emmons et al., 2010). Tropospheric chem-

215   istry is represented by 81 chemical species, which participate in 38 photolysis and 159 gas-phase

216   reactions. The MOZART- 4 mechanism includes explicit representation of the NMVOCs ethane,

217   propane, ethene, propene, methanol, isoprene, and α-pinene. Other NMVOC species are represented

218   by lumped species based on the reactive functional groups. In the WRFV3.5.1 code, two bug fixes

219   have been included for the MOZART- 4 mechanism: the NH_3+OH rate coefficient has been cor-

220   rected following Knote et al. (2015), and a correction has been made to treatment of the vertical

221   mixing of MOZART- 4 species (A.K. Peterson, personal communication). In the WRF-Chem sim-

222   ulations, we use the version of MOZART- 4 coupled to the simple GOCART aerosols mechanism

223   (Ackermann et al., 1998b), known as the MOZCART mechanism. In this paper, we limit our anal-

224   ysis to gas-phase species. Because of this focus, and to simplify the interpretation the mechanism

225   intercomparison (see below), all aerosol radiative feedbacks (i.e., both direct and indirect effects) are

226   turned off in all model simulations in this study.

227   In the RADM2 simulation, gas phase chemistry is represented by the second generation Regional

228   Acid deposition Model (RADM2) (Stockwell et al., 1990). This mechanism has 63 chemical species

229   which participate in 21 photolysis and 136 gas phase reactions. The NMVOC oxidation in RADM2 is

230   treated in a less-explicit fashion than in MOZART, in which ethane, ethene and isoprene are the only

231   species treated explicitly and all other NMVOCs are assigned to lumped species based on OH reac-

232   tivity and molecular weight. In WRF-Chem, RADM2 is coupled to the MADE/SORGAM aerosol

233   module, which is based on the Modal Aerosol Dynamics Model for Europe (MADE) (Binkowski

234   and Shankar, 1995; Ackermann et al., 1998a) and Secondary Organic Aerosol Model (SORGAM)

235   (Schell et al., 2001). However, as noted above, in this study we focus our analysis on gas-phase

236   chemistry.

237   In both the RADM2 and MOZART simulations, the chemical mechanism code was generated

238   with the Kinetic Pre-Processor (KPP) (Damian et al., 2002; Sandu and Sander, 2006), and equations

239   are solved using a Rosenbrock-type solver. Note that when using RADM2 chemistry, there are two

240   different solvers available within WRF-Chem. We chose to use the KPP chemistry and Rosenbrock

241   solver to be consistent with the MOZART runs, and also because the alternative QSSA chemistry

242   solver has been shown to have problems representing NO_x titration (Forkel et al., 2015). In partic-

243   ular, the QSSA treatment of RADM2 chemistry was found to result in an under-representation of

244   nocturnal ozone titration for areas with high NO emissions.

3 Observational datasets

A summary of the observational datasets used for model evaluation can be found in Table 3.

3.1 Meteorology

Since WRF-Chem couples the meteorology simulations online with the chemistry, we begin by evaluating the modeled meteorological fields against observations which are driving the simulations of chemical fields. In this study, the WRF-Chem simulated meteorological fields are evaluated against the in situ measurements of mean sea level pressure (MSLP), 2-meter temperature (T2) and 10-meter wind speed and direction (WS10 and WD10, respectively) from the Global Weather Observation dataset provided by the British Atmospheric Data Center (BADC). We chose these meteorological variables for the evaluation as these are expected to have the most significant influence on the gas-phase chemistry, which is the main focus of this study.

3.2 Chemistry

3.2.1 EMEP Network

The EMEP observational dataset provides surface measurements of pollutant concentrations, including tropospheric ozone and its precursors, at stations chosen to be representative of regional background pollution (see, e.g., Tørseth et al., 2012). The regional focus is in keeping with the goals of the Convention on Long-range Transboundary Air Pollution (CLRTAP), under which this network is administrated.

3.2.2 AirBase Network

AirBase is the public air quality database of the European Environmental Agency (EEA), and represents a much denser network of monitoring than the EMEP network (http://www.eea.europa.eu/data-and-maps/data/airbase-the-european-air-quality-database-7). Because of the relatively coarse horizontal resolution in this model study, model output is only compared against AirBase stations that are classified as "rural background." The station classification was taken from the metadata provided by the EEA for AirBase. Some AirBase stations are also part of the EMEP network; the subset of AirBase stations used in this study exclude any stations that are also part of the EMEP network (since they are already included in the evaluation against EMEP observations).

3.3 Evaluation methodology

Stations were excluded from our season-by-season analysis if the temporal coverage was less than 75%, i.e., if missing or flagged hourly (or 3-hourly) data represented more than 25% of the hourly (or 3-hourly) time series over the entire season. For sensitivity studies that consider the month of

276   July only, stations were considered that had at least 75% temporal coverage for the month. This
277   criteria was applied for all meteorological and chemistry observations. For comparison of model
278   output to in situ observations, the model gridcell that is closest to the latitude, longitude location
279   of the measurement station was chosen. Statistics calculated include the mean, mean bias (MB),
280   normalized mean bias (NMB), mean fractional bias (MFB) and the temporal correlation coefficient
281   (r). The domain-wide statistics presented in Tables 4 - 9 were calculating by first calculating the
282   statistical quantity hour-by-hour at each station, and then averaging these values over all times (in
283   the season) and all stations. Definitions of calculated statistical quantities can be found in Appendix
284   B. When applying these statistics to wind direction, wind direction was treated as a scalar quantity,
285   when in fact it is a vector. This simple approach was favored rather than applying a correction (as
286   done by, e.g., Zhang et al. (2013a) in cases where the difference in modeled vs. observed wind
287   direction were greater than $180°$). This is not expected to make an important impact on our analysis,
288   especially since northerly winds (i.e., centered around $0°$, or equivalently $360°$) are not prevalent in
289   Europe (see Figure 3 and Figure S2 in the Supplementary Material).

290   From hourly concentrations of O_3, both observed and modeled, additional ozone metrics for
291   health impacts are calculated. MDA8 is defined as the maximum daily 8-hour mean ozone, in ac-
292   cordance with the European Union's Air Quality Directive. Note that, for calculation of MDA8,
293   a missing value was assigned if one or more hours of data in the 8-hour average were missing.
294   SOMO35 is an indicator of cumulative annual ozone exposure used in health impact assessments.
295   The accumulated health impact is assumed to be proportional to the sum of concentrations above
296   a cutoff of 35 ppb, chosen because the relationship between O_3 and adverse effects is very uncer-
297   tain below this threshhold (WHO, 2013). Mathematically, SOMO35 is defined as the sum of MDA8
298   levels over 35 ppb ($70\,\mu g\,m^{-3}$) over a year, in units of concentration·days, following Amann et al.
299   (2008).

300   $$SOMO35 = \frac{365}{N_{valid}} \sum_{iday} max(0, C_{iday} - 70\,\mu g\,m^{-3})$$

301   where N_{valid} is the number of valid (i.e., non-missing) daily values.

302 **4   Results and Discussion**

303 **4.1   Evaluation of Meteorology**

304   Table 4 shows a summary of domain-wide statistics evaluating the MOZART model simulation
305   against observations of meteorological variables MSLP, T2, WS10 and WD10; the spatial distri-
306   bution of these statistics shown in Figures 1-3 for temperature and wind variables. Differences in
307   predicted meteorology between the MOZART and RADM2 simulations are small, with differences
308   in MSLP less than one hundredth of 1%, and differences in T2, WS10, and WD10 generally far
309   below 1%. Since the simulations were run without aerosol-radiative feedbacks, it was expected that

the two simulations would show minimal differences in meteorology, and we conclude that differences in O_3 and NO_x predicted in the MOZART and RADM2 simulations (Section 4.2) are a direct result of differences in the chemistry, rather than chemistry-radiative feedbacks. Statistics for meteorology for the RADM2 simulation can be found in the Supplementary Material, Table S1 and Figures S4-S7.

MSLP has been reproduced over the entire European domain with a high degree of skill in every season for both simulations, with negligible bias (domain-averaged NMB and MFB are zero in all seasons) and temporal correlation coefficients (r values) of 0.98 or greater (see also Figures S3 and S7 in the Supplementary Material).

The spatial distribution of seasonal average T2 in the model and observations is shown in Figure 1, along with the spatial variation in mean bias and temporal (3-hourly) correlation. Overall, the spatial variability in measured T2 is found to be well-reproduced by WRF-Chem during all the seasons. The absolute values of mean biases in T2 were generally found to be lower than $1°$ C. Larger biases in T2 can be found in the Alps, in particular during winter, where T2 is often overpredicted by more than $1°$ C (Figure 1). This larger bias over mountainous regions, also found in a previous study (Zhang et al., 2013a), is likely due to the complex mountain terrain and related unresolved local dynamics. The r values are generally found to be more than 0.9 in all the seasons and show no significant geographical variation, indicating that the model is able to reproduce the hourly variations in near surface temperature. Averaged over the entire domain, the mean bias in T2 varies from -0.4 to + $0.3°$ C depending on the season (Table 4).

The spatial variability in wind speeds, including the seasonality, with strongest winds during the winter, have been reproduced by the model (Figure 2). However, the model tends to overestimate winds speeds with larger biases (2 m/s or more) during the winter and fall. The regions showing greater bias in wind speed include the Alps, coastal regions, and the low-lying areas of northern Germany and Denmark (Figure 2). The temporal correlation of wind speed is generally above 0.7 in the northern half of the domain, but is lower (0.4-0.6) in the southern part of the domain, in areas in the Alps and close to the Mediterranean (Figure 2). Similar behavior for modeled wind speed is reported by Zhang et al. (2013a), who attributes the overestimation in wind speeds primarily to poor representation of surface drag exerted by unresolved topographical features, which results in model limitations in simulating circulation systems such as sea breeze and bay breeze. An overview of the statistics for wind direction is presented in Table 4, with the spatial distribution shown in Figure 3. Wind direction over the continent is predominantly from the west and south, and the mean bias in wind direction is between 20 and 30 degrees depending on the season. Similar to the patterns seen for wind speed, areas with complex topography (the Alps, the Balkans, the Mediterranean coast) show the largest biases and the lowest correlations for wind direction.

345   Overall, we find that WRF-Chem is capable of reproducing the spatial and temporal variations

346   in the European meteorological conditions reasonably well, in a manner consistent with previous

347   studies (e.g. Zhang et al., 2013a).

4.2   Evaluation of Chemistry

4.2.1   Ozone

350   We begin the evaluation of chemistry by examining the seasonal average surface O_3 distribution

351   over Europe from the MOZART simulation, as shown in Figure 4. Predicted surface O_3 distributions

352   show a clear seasonality, with maximum concentrations during summer. In all seasons, surface O_3

353   concentrations are highest over the Mediterranean region, with values during the spring and summer

354   greater than 110 $\mu g \, m^{-3}$. Simulated concentrations reproduce the north-south gradient in O_3 seen

355   in the ground-based observations. Figure 5 provides another comparison of seasonal average O_3

356   distributions in the model vs. the observations (from both the AirBase and EMEP networks) and

357   additionally shows the spatial distribution of MB and r, the temporal (hourly) correlation coefficient;

358   performance statistics are shown in Table 5 (against observations from the AirBase network) and

359   Table 6 (against observations from the EMEP network). MOZART overpredicts O_3 concentrations

360   for most of Europe in the summer and fall. In winter and spring, MOZART tends to underestimate O_3

361   in north-central Europe, but overestimate O_3 in southern Europe. Hourly correlation coefficents for

362   O_3 are highest (greater than 0.6) in northern Europe (especially France, Germany, and the Benelux

363   region) and in Spain, but are lower (with values of approximately 0.4) throughout Italy and the

364   mountainous regions of the Alps. Notably, Italy and the Alps are the regions within our domain

365   that exhibit the highest biases and lowest correlations with respect to wind direction and speed

366   (Section 4.1), which could explain the poorer temporal correlation for O_3 in these areas.

367   Looking at Tables 5 and 6, we see some differences in the statistical performance of the MOZART

368   simulation when compared to the EMEP vs. the AirBase observational datasets. Considering the

369   EMEP observations over the whole domain (Table 6), MOZART slightly overpredicts O_3 in sum-

370   mer, with a summertime mean bias of 4 $\mu g \, m^{-3}$, whereas the summertime mean bias when compared

371   the AirBase network is 10 $\mu g \, m^{-3}$ (Table 5). In winter and spring, the bias (MB, NMB, and MFB)

372   in MOZART-predicted O_3 is more negative when compared to EMEP observations than to AirBase

373   observations. In fall, the sign of the domain-average bias changes if considering the model perfor-

374   mance against EMEP vs. AirBase observations. These differences likely reflect differences in the

375   character of the two observational networks. First, we expect that the Airbase rural background sites

376   considered here may be, on average, more influenced by local pollution sources than the EMEP

377   sites, which are selected to be representative of more remote regional background. Secondly, the ge-

378   ographical coverage of AirBase vs. EMEP sites for O_3 is slightly different (Figure S8). In particular,

379   coverage of the U.K. and the Nordic countries is almost exclusively via the EMEP network, poten-

380 tially giving the EMEP observations a northern bias in comparison to the AirBase-only sites. Both

381 features of the measurement networks could explain the lower values of the domain-wide average

382 O_3 observed at the EMEP vs. the AirBase stations.

383   In addition to evaluating the model's ability to simulate hourly O_3 concentrations, we also con-

384 sider MDA8 and SOMO35, two metrics designed to evaluate the impact of ozone on health. The

385 distribution of seasonal average values of MDA8 is shown in Figure 6 for the MOZART simulation.

386 The European Union's Air Quality Directive states that, as a long-term objective, MDA8 should not

387 exceed the threshhold value of $120\,\mu g\,m^{-3}$; as a target value this long-term objective should not be

388 exceeded on more than 25 days per year, averaged over 3 years. Figure 6 shows that, at some stations

389 in the Alps and in southern Italy during summer, the average value of MDA8 exceeds $120\,\mu g\,m^{-3}$.

390 As seen in Figure 7, the number of days when MDA8 exceeds the $120\,\mu g\,m^{-3}$ is greater than 25 in

391 spring alone for much of southern Europe, which is also captured well by the MOZART simulation.

392 MOZART tends to overpredict MDA8 and the days in exceedance of the target value in summer and

393 fall, consistent with the overestimation of hourly average O_3 during this season. Since the metric

394 MDA8 is, in effect, a measure of daytime ozone, it is always higher than the straight average of

395 hourly concentrations. As a consequence, MOZART shows greater bias in MDA8 than in average

396 O_3 in seasons where average O_3 is already overpredicted (Tables 5 and 6). In general, regional and

397 seasonal patterns for MDA8 simulated by MOZART are similar to those for simulated average O_3.

398 SOMO35, an indicator for cumulative annual exposure, is shown in Figure 8 for the year 2007.

399 MOZART is able to reproduce the north-south gradient of SOMO35 seen in the observations quite

400 well, while overpredicting the magnitude of SOMO35 by $2\,mg\,m^{-3}\cdot days$ (Table 7).

401   WRF-Chem simulations using the RADM2 chemical mechanism show a spatial and seasonal

402 distribution of surface O_3 over Europe (Figures 9 and 10) that is qualitatively similar to that for

403 MOZART. The correlation coefficients for the MOZART and RADM2 simulations are also similar

404 in both magnitude in distribution (Figures 5 and 10. Absolute O_3 concentrations are most similar

405 (i.e., less than 5% different) between the mechanisms near the northwest edges of the domain (see

406 Figures 4 and 9), where the prevailing westerly winds (Supplementary Material, Figure S2) mean

407 that O_3 imported from the boundary conditions plays a dominant role. However, it is striking to

408 note that the surface O_3 concentrations predicted by two different chemical mechanisms are gen-

409 erally quite different, with RADM2 predicting average surface O_3 values that are approximately

410 $20\,\mu g\,m^{-3}$ lower than those predicted by MOZART in spring and summer (c.f. Figures 4 and 9,

411 Tables 5 and 8, and Tables 6 and 9). In contrast to MOZART, RADM2 underpredicts O_3 through-

412 out most of Europe in all seasons. An exception to this is in southern Europe in winter, where

413 RADM2, like MOZART, shows some overprediction of O_3 concentrations in southern Europe, par-

414 ticularly near the Mediterranean. RADM2 also overpredicts O_3 near the Mediterranean in fall (a

415 season where MOZART overpredicts O_3 Europe-wide). The general underprediction of O_3 con-

416 centrations in RADM2 means that the health metrics MDA8 and SOMO35 are also underpredicted

417 (Tables 7- 8 and Figure 8). Overall, absolute biases (i.e., the absolute value of MB, NMB, and MFB)

418 are smaller for MOZART than for RADM2, indicating that MOZART is more successful overall in

419 reproducing European ground-level O_3.

420 Model biases for O_3 in both the MOZART and RADM2 simulations are in line with biases found

421 in other regional modeling studies for Europe. For instance, values for the NMB in European sum-

422 mertime O_3 ranged from less than -20% to greater than +20% depending on the ensemble member

423 in AQMEII (Solazzo et al., 2012b; Im et al., 2015), compared to values of -18% and +14% for the

424 RADM2 and MOZART simulations, respectively, in the present study. Zhang et al. (2013b) found

425 domain-wide values for NMB for O_3 ranging from +4.2% to +19.1% for the month of July 2001,

426 depending on their model configuration. Tuccella et al. (2012) report a domain-average mean bias in

427 O_3 of -1.4 $\mu g\,m^{-3}$ averaged over the whole year. Although the work of Tuccella et al. (2012) uses

428 the RADM2 chemical mechanism and simulates the year 2007, similar to the RADM2 simulation in

429 the present study, there are several differences in model configuration that could explain the observed

430 differences in predicted O_3, including the use of time-invariant chemical boundary conditions, the

431 use of the QSSA rather than the Rosenbrock chemical solver (which has been shown to make a

432 difference Forkel et al. (see 2015)), and the use of an alternate emissions inventory (from EMEP).

433 The temporal correlation with hourly measurements for O_3 in this study are also in line with

434 other regional modeling studies of O_3 for Europe. Simulations with both chemical mechanisms lead

435 to reasonable correlations between the model-predicted and observed O_3 concentrations over the

436 entire domain, with r values generally in the range of 0.6-0.8 (Figures 5 and 10, Tables 5 and 8).

437 This is consistent with the hourly correlation coefficient for O_3 of 0.62 reported by Tuccella et al.

438 (2012), where their r value represents an average over the entire year of 2007. Zhang et al. (2013b)

439 also report correlation coefficients of 0.6-0.7 for hourly O_3 over the European domain (horizontal

440 resolution 0.5°) using the CB05 gas-phase chemical mechanism in WRF-Chem.

441 In addition to evaluating the performance of the MOZART and RADM2 simulations on their abil-

442 ity to reproduce ground-level ozone concentrations, we compare the observed sensitivity of modeled

443 O_3 to the choice of chemical mechanism to other studies that have investigated the uncertainty in 3-D

444 model predictions associated with the choice of chemical mechanism. Knote et al. (2015) used box

445 model simulations based on AQMEII phase 2, and concluded that the uncertainty in predicted O_3 in

446 a 3-D model solely due to the choice of gas phase chemical mechanism should be of the order of 5%,

447 or 4 $ppbv$ (8 $\mu g\,m^{-3}$). This is quite a bit smaller than the sensitivity to chemical mechanism found

448 in this study, where we see differences in summertime average O_3 of 20 $\mu g\,m^{-3}$, corresponding to a

449 relative difference of approximately 40%. Coates et al. (2016) have shown that adding representation

450 of stagnant conditions (which were not represented in Knote et al. (2015)) to a box model increased

451 the sensitivity of predicted O_3 to the chemical mechanism, and also improved model agreement

452 with observations. This result suggests that day-to-day variability in meteorological conditions and

453 transport can enhance the sensitivity of O_3 to chemical mechanism compared to what is seen in box
454 models.

455   Another interesting basis for comparison is the study of Mallet and Sportisse (2006), who investi-
456 gate uncertainty in the CTM Polyphemus due to various physical parameterizations, including chem-
457 ical mechanism (comparing RACM and RADM2), using an ensemble approach. They estimated an
458 overall uncertainty in O_3 concentrations of 17% based on choices for physical parameterizations in
459 general, but identifed the choice of chemical mechanism along with the turbulent closure parame-
460 terization as the two most important drivers of this uncertainty. Simulations using the RACM vs.
461 RADM2 mechanisms yielded differences in average O_3 concentrations of 7-13 $\mu g\, m^{-3}$, depending
462 on the other parameterizations used. It is clear that the sensitivity of O_3 to the use of the MOZART
463 vs. RADM2 chemical mechanism in this study is large compared to other studies of mechanism
464 comparisons in 3-D models (see also Luecken et al., 2008; Kim et al., 2010)), though even larger
465 absolute differences in hourly O_3 concentrations (up to 40 ppb, or 80 $\mu g\, m^{-3}$) have been found in
466 studies of episodic ozone (Faraji et al., 2008; Yarwood et al., 2003). It is possible that MOZART
467 and RADM2 as implemented in this study are examples of chemical mechanisms that are extremely
468 different from one another on a spectrum of other commonly-used mechanisms; the differences be-
469 tween the two mechanisms will be further explored in Section 4.3.

470 ### 4.2.2   Nitrogen oxides

471 Seasonal average surface-level NO_x for the MOZART simulation are shown in Figure 11. Several
472 hotspots in the spatial distribution of NO_x mixing ratios are apparent, as expected based on the
473 intensity of emissions in these areas. NO_x hotspots with concentrations of more than 30 $\mu g\, m^{-3}$
474 are visible over parts of France, Belgium, Germany and Russia. Similar high concentrations are
475 also seen over the marine regions close to Barcelona, Monaco, and southern France. As shown
476 in Table 5, the MOZART simulation slightly underpredicts domain-average NO_x concentrations
477 for all seasons when comparing to AirBase observations. In Figures 12 and 13 we examine the
478 spatial distribution of NO_x broken down into its components, NO_2 and NO, together with the spatial
479 distribution of MB and r. The MOZART simulation overestimates NO_2 in the U.K., northern France,
480 Belgium, and central Germany, all of which are regions known for having high NO_x emissions and
481 concentrations. However this does not hold true for the Netherlands, a neighboring region with high
482 emissions where MOZART tends to underpredict rather than overpredict NO_2 concentrations. NO,
483 on the other hand, is significantly underpredicted compared to surface measurements throughout
484 the domain. This may be partially due to the relatively coarse horizontal resolution of the model, in
485 which fresh NO emissions are immediately diluted over a large area, and could also be a consequence
486 of model deficiencies in representing NO_x chemical cycles. Artifacts related to reporting of low
487 NO concentrations approaching measurement detection limits could also play a role (observed time

488   series for NO typically show a baseline of 1-2 $\mu g \, m^{-3}$, whereas modeled concentrations reach a

489   baseline of zero).

490   Domain average temporal correlation coefficients (r) against hourly measurements of NO_x, NO_2,

491   and NO (Tables 5 and 6) range from approximately 0.2 to 0.5, which is lower than correlations for

492   O_3 but consistent with other studies, dicussed further below. In all seasons, the domain-averaged

493   temporal correlation coeffiecient is higher when compared to EMEP vs. AirBase observations. This

494   is attributed to lesser local influences and therefore better regional representativeness of the EMEP

495   stations. No exceptional patterns are seen in the spatial distribution of r for NO_2 or NO, although

496   correlation appears slightly better in the northern part of the domain. The MOZART simulation

497   shows the highest domain-average correlation coefficients (r) for NO_x, NO_2, and NO in winter and

498   fall, and the lowest domain-average r values in summer.

499   NO_x predicted by the RADM2 simulation shows fairly similar behavior to NO_x predicted by

500   the MOZART simulation (cf. Figures 12 and 14 and additional Figures S10-S11 in the Supple-

501   mentary Material). In general, simulated NO_x concentrations are slightly higher for MOZART than

502   for RADM2. Domain-wide average NO_x concentrations predicted by MOZART are approximately

503   2 $\mu g \, m^{-3}$ higher than for RADM2 in all seasons except winter, where the difference is approximately

504   3 $\mu g \, m^{-3}$ (cf. Tables 5 and 8). The spatial distribution of MB for NO_2 for the RADM2 simulation

505   generally shows the same patterns as observed for the MOZART simulation, namely a slight over-

506   estimation in the U.K., northern France, Belgium, and central Germany. Like for MOZART, NO

507   for RADM2 is underpredicted throughout the domain, with NO concentrations slightly more neg-

508   atively biased than in MOZART in all seasons except Fall, when NO concentrations are higher for

509   RADM2 than for MOZART and show better agreement with the observations. Temporal correlation

510   for NO_2 and NO in RADM2 is also found to show similar behavior to the MOZART simulation.

511   An exception to the similarity observed between the mechanisms for NO_x can be seen over central

512   Germany in winter, where MB values for NO_2 are 6-10 $\mu g \, m^{-3}$ for MOZART (Figure 12), but in the

513   range of 0-6 $\mu g \, m^{-3}$ for RADM2 (Figure 14). Differences in NO_x concentrations predicted by the

514   MOZART vs. RADM2 simulations are generally less than 20%, consistent with Knote et al. (2015),

515   who conclude that uncertainty due to choice in chemical mechanism leads to an uncertainty of up to

516   25% in 3-D model simulations.

517   Performance of the present simulations with respect to NO_2 can also be compared to previous

518   published studies (note that none of the above-cited studies perform a validation for NO or NO_x).

519   Zhang et al. (2013b) reports NMB values of approximately -15% for NO_2 for WRF-Chem simu-

520   lations against hourly AirBase measurements for July 2001, in line with values of -12% and -19%

521   for the MOZART and RADM2 simulations in this study, respectively. Tuccella et al. (2012) report a

522   MB for NO_2 of -0.9 $\mu g \, m^{-3}$ averaged over the whole year; for comparison the RADM2 simulation

523   in this study shows a MB in the range of -2.5 to -1 $\mu g \, m^{-3}$ for fall, spring and summer, but a MB of

524 +0.67 $\mu g\,m^{-3}$ in summer. Evaluation of NO_2 was not treated in detail in the AQMEII studies, but

525 Im et al. (2015) report that the models for the European domain underestimate NO_2 by 9% to 45%.

4.3 Characterization of MOZART vs. RADM2 differences

527 In this section, we explore the differences in surface O_3 between the MOZART and RADM2 simula-

528 tions by examining net O_3, NO_2, and NO production rates as well as the NO_x- and VOC-sensitivity

529 of the two mechanisms. We further conducted sensitivity simulations to investigate the relative con-

530 tributions of different sources to the observed differences in surface O_3 predicted by MOZART and

531 RADM2. The month of July was chosen for the sensitivity simulations since O_3 concentrations over

532 Europe are highest during summer, and thus summer is most the most important season when con-

533 sidering air quality exceedances and health impacts of O_3. Additionally, MOZART and RADM2

534 show the largest differences in predicted O_3 during this season (see Tables 5 and 8).

535   To gain insight into model behavior for O_3, we added terms to the model output representing

536 hourly accumulated tendencies, i.e., the change in concentration of a species due to photochemistry

537 only, for July simulations using MOZART and RADM2. The hourly net photochemical production

538 rate was calculated as the difference in the accumulated tendency from one timestep to another. Fig-

539 ure 15 shows the average of the midday (11:00-14:00 CEST, or 9:00-12:00 UTC) photochemical

540 production rate of O_3 and NO_x components for both the MOZART and RADM2 simulations. (Note

541 that the net photochemical production rate is shown here in $ppb\,hr^{-1}$ for more intuitive comparison

542 of production and loss of the different species on a mole basis; $\mu g\,m^{-3}$ was used in Section 4.2 be-

543 cause this is the unit in which limit and target values in the EU Air Quality Directive are expressed.)

544   Overall, the spatial variability as well as the magnitudes of net O_3 production rates are found to

545 be similar for MOZART- 4 and RADM2 chemistry (Figure 15). For both mechanisms, the greatest

546 midday net O_3 production rates are found in southern Europe, particularly over the Mediterranean

547 and Atlantic coasts. The difference in net O_3 production rate between the two mechanisms is also

548 shown in Figure 15. MOZART exhibits greater net O_3 photochemical production rates than RADM2

549 for most of Europe, with the exception of the southeast corner of the domain (Greece, Turkey, and

550 the nearby Mediterranean), where net O_3 production rates are greater for RADM2. The difference

551 in net O_3 production rate (MOZART-RADM2) shows a large maximum over central Europe, cen-

552 tering over Germany and extending west and east into France and Poland. Over Germany, net O_3

553 production in MOZART is seen to be higher than in RADM2 by 1.8 $ppb\,hr^{-1}$ or more.

554   As expected, regions of high NO_2 production in both MOZART and RADM2 simulations are seen

555 over the high NO_x-emission regions including Benelux, southern England, western Germany, the

556 Po Valley, and major cities including Paris and Moscow. The difference in net NO_2 production rate

557 between the two mechanisms is also highest where the absolute NO_2 production rates are highest;

558 in these areas the net NO_2 production rate is lower for MOZART than for RADM2 by greater than

559 0.25 $ppb\,hr^{-1}$. Furthermore, areas where the two mechanisms show the greatest differences in net

560   NO_2 production rate tend to be the areas where the net O_3 production rate is most different between

561   the two mechanisms, including the large maximum over the Netherlands and northwest Germany.

562   To further investigate the differences between ozone chemistry in MOZART vs. RADM2, we

563   performed two additional sensitivity studies with each mechanism: one in which all anthropogenic

564   NO_x emissions were increased by 30%, and one in which all anthropogenic VOC emissions were

565   increased by 30%. We then examined the change in O_3 concentrations due to these emission per-

566   turbations to diagnose whether the chemical mechanisms were operating in a NO_x-sensitive or a

567   VOC-sensitive regime. Results are shown in Figure 16. For the simulations where NO_x emissions

568   were increased by 30%, MOZART and RADM2 show very similar behavior. Most of the domain

569   is NO_x sensitive, with increased NO_x emissions resulting in increased modeled O_3. Notably, the

570   U.K., Benelux, northern France and Paris, and northwest Germany show NO_x-saturated behavior,

571   in which increased NO_x emissions lead to decreased O_3 concentrations. NO_x-saturated regimes are

572   also seen around the area of the Mediterranean between Monaco, Genoa and Corsica. An alternate

573   approach to identify areas of NO_x-sensitive vs. NO_x-saturated regimes is to use indicator ratios (in

574   the base simulation) following Sillman (1995). We have applied this approach with the indicator ratio

575   CH_2O/NO_y (Figure S12) and find that areas identified as NO_x sensitive using the indicator ratio are

576   the same as those identified using the simulation with +30% NO_x emissions. These results are also

577   consistent with the areas of Europe found to be NOx saturated in the model study of Beekmann and

578   Vautard (2010). Magnitudes of the observed change in O_3 in response to increased NO_x emissions

579   are quite similar for both mechanisms, although RADM2 shows slightly stronger NO_x saturation

580   (i.e., a stronger decrease in O_3 given a 30% increase in NO_x emissions) in the area centered around

581   Benelux, and stronger NO_x sensitivity over Scandinavia and northwest Russia.

582   In contrast to the similar behavior seen for NO_x sensitivity, the VOC sensitivity exhibited by the

583   two mechanisms is quite different (Figure 16, lower panel). For both MOZART and RADM2, the

584   effect of increased anthropogenic VOC emissions on O_3 is smaller than the effect of increased NO_x

585   emissions. The MOZART simulation shows very little impact of increased VOC emissions on O_3,

586   with differences in average O_3 concentration generally confined to $\pm$ 2% of the base simulation.

587   In contrast, increasing VOC emissions in the RADM2 simulations leads to increased O_3 concentra-

588   tions throughout nearly the entire domain. Areas where MOZART and RADM2 are in agreement in

589   predicting VOC sensitivity (increased O_3 concentrations in response to increased VOC emissions)

590   are generally those with high NO_x emissions, where one would expect the highest VOC sensitivity

591   based on theory; these areas include Benelux, northern France, northwest Germany, and shipping

592   tracks in the Mediterranean. However, the increase in O_3 concentration is modest for both mecha-

593   nisms; for RADM2 it is generally limited to increases of 2-4% over the base simulation. The results

594   of the +30% VOC sensitivity studies for July indicate that $d[O_3]/d[VOC]$ is higher (more positive)

595   for RADM2 than for MOZART for the chemical regime represented by the models in July 2007.

596   This shows that the two mechanisms are simulating different O_3 chemical regimes – in the case of

597   RADM2, there is greater VOC sensitivity, meaning that addition of VOC emissions moves the chem-
598   istry in the direction of maximum O_3 production efficiency; this is not the case for MOZART over
599   much of the domain. A more extensive study would be needed to evaluate whether the conclusion
600   that $d[O_3]/d[VOC]$ is higher for RADM2 than for MOZART can be applied more generally.

601   Taken as a whole, Figure 16 shows that MOZART behaves in a classically NO_x-sensitive manner
602   for most of domain, with O_3 responding to changes in NO_x but showing little response to changes
603   in anthropogenic VOC. NO_x-saturated behavior is also observed, particularly around the area of
604   U.K., Benelux, and northern France and Germany. RADM2, on the other hand, exhibits more of
605   a mixed NO_x- VOC-sensitivity for much of the domain. The NO_x sensitivity seen in RADM2 is
606   very similar to that seen in MOZART, but the response of RADM2 to changes in VOC is much
607   stronger (by about a factor of two) than observed in MOZART. With the exception of some small
608   areas in the North and Baltic Sea south of Norway and Sweden, RADM2 predicts O_3 increases
609   with VOC increases throughout the entire domain. This difference in VOC sensitivity seen between
610   the mechanisms has implications for policy decisions, as it indicates uncertainty in the European
611   response of O_3 to policies designed to reduce anthropogenic VOC emissions.

612   In addition to characterizing mechanism behavior with respect to net photochemical O_3 produc-
613   tion and NO_x- and VOC-sensitivity, we evaluate the contribution of other sources that could ex-
614   plain the large differences in predicted O_3 between the MOZART and RADM2 simulations. First,
615   MOZART and RADM2 use different rate coefficients for several inorganic gas phase chemical re-
616   actions. To test the effect of these differences, all RADM2 inorganic reaction rate coefficients were
617   changed so that they matched those used in MOZART simulations in the cases where the reactions
618   are the same in both mechanisms (Section S3 in the Supplementary Material). The differences in
619   inorganic rate coefficients between the two mechanisms explain a significant difference in predicted
620   O_3 concentrations: when RADM2 is run with inorganic rate coefficients from MOZART, the result-
621   ing domain-mean O_3 is higher by more than $8\,\mu g\,m^{-3}$ for the month of July, approximately 40% of
622   the difference in predicted O_3.

623   Besides the gas-phase chemistry itself, there are some differences in the implementation of MOZART-
624   4 vs. RADM2 in WRF-Chem that could also contribute to the observed differences in modeled O_3:
625   in particular, in the treatment of dry deposition and photolysis (described in the Supplementary Ma-
626   terial, Section S2). To test the effect of differences in treatment of dry deposition, we conducted
627   an additional sensitivity in which we modified the RADM2 simulation to treat dry deposition in
628   the same way as it is treated in MOZART. However, this led to only a small difference in average
629   ozone (an increase of $1\,\mu g\,m^{-3}$), indicating that modeled surface O_3 concentrations are relatively
630   insensitive to these differences in the treatment of dry deposition, at least in the summer. In a sen-
631   sitivity test where we modified the model code so that the MOZART simulation ran with the same
632   photolysis scheme as used in our RADM2 simulation (i.e., with the Madronich TUV scheme and
633   without reading in climatological O_3 and O_2 columns), we found that average O_3 for July decreases

634   by $3\,\mu g\,m^{-3}$. This indicates that modeled O_3 is also somewhat sensitive to differences in the treat-

635   ment of photolysis in MOZART and RADM2. However, taken together, our sensitivity simulations

636   suggest that the differences in the inorganic reaction rate coefficients are more important than the

637   differing treatments of dry deposition and photolysis in explaining the differences in predicted O_3

638   between the RADM2 and MOZART simulations.

639   ## 5 Summary and Conclusions

640   In this paper, we present a detailed description of a WRF-Chem setup over the European domain

641   and provide an evaluation of the simulated meteorological and chemical fields with an emphasis

642   on model's ability to reproduce the spatial and temporal distribution of ground-level O_3 and NO_x.

643   Within WRF-Chem we compare the performance of two different chemical mechanisms: MOZART-

644   4, for which we present the first model evaluation for a European domain, and RADM2. Overall, we

645   found that our WRF-Chem setup reproduced the spatial and seasonal variations in the meteorological

646   parameters over Europe, with biases and correlations consistent with previous studies. Simulations

647   using the MOZART- 4 as well as RADM2 chemical mechanisms were found to reproduce the spatial

648   and temporal distributions in ground-level O_3 over Europe, based on observations from the EMEP

649   and Airbase networks. However, we find significant differences in O_3 concentrations predicted by the

650   two chemical mechanisms, with RADM2 predicting as much as $20\,\mu g\,m^{-3}$ less O_3 than MOZART

651   during the spring and summer seasons. In general, MOZART- 4 chemistry overpredicts O_3 concen-

652   trations for most of Europe in the summer and fall, whereas RADM2 leads to an underestimation of

653   O_3 over the European domain in all seasons. Taken as a whole, use of MOZART- 4 chemistry per-

654   forms better, leading to lower absolute model biases in O_3. This is the case when considering hourly

655   O_3 concentrations as well as metrics relevant for human health, such as MDA8 and SOMO35. De-

656   spite the large differences in predicted O_3, the two mechanisms show relatively similar behavior for

657   NO_x, with both MOZART and RADM2 simulations resulting in a slight underestimation of NO_x

658   compared to surface observations.

659   The net midday photochemical production rate of O_3 in summer is found to be higher for MOZART

660   than for RADM2 for most of the domain, with the largest differences between the mechanisms seen

661   over Germany, where the net O_3 photochemical production for MOZART is higher than for RADM2

662   by greater than $1.8\,ppb\,hr^{-1}$ ($3.6\,\mu g\,m^{-3}\,hr^{-1}$). However, we have shown that RADM2 is approx-

663   imately twice as sensitive to increases in anthropogenic VOC emissions as MOZART, suggesting

664   that, under local VOC-limited conditions not seen at the regional scale of our simulations, RADM2

665   is likely to produce O_3 at a greater rate than MOZART. Despite the differences in sensitivity to

666   changes in VOC emissions exhibited by the two mechanisms, sensitivity to changes in NO_x emis-

667   sions in MOZART and RADM2 are found to be similar.

668   Our results indicate that modeled surface O_3 over Europe is sensitive the choice of gas phase

669   chemical mechanism, with observed differences in O_3 between mechanisms that are larger than

670   those seen in many past studies. Although the most fundamental differences between MOZART- 4

671   and RADM2 (and other chemical mechanisms used in regional modeling) is the representation of

672   VOC oxidation chemistry, we find that approximately 40% of the difference seen in predicted O_3

673   seen in this study can be explained by differences in inorganic reaction rate coefficients employed

674   by MOZART- 4 and RADM2. This result suggests that harmonization of inorganic rate coefficients

675   among chemical mechanisms used for regional air quality modeling might be valuable, and could

676   potentially lead to a smaller spread in model-predicted O_3 compared to that seen in, e.g., the multi-

677   model studies of AQMEII (Solazzo et al., 2012b; Im et al., 2015). Further investigation of chemical

678   mechanism behavior within 3-D models in general would be helpful to constrain uncertainties in

679   regional air quality modeling.

6   Code availability

681   The WRF-Chem model is an open-source, publicly available software. The code is being continually

682   improved, with new releases approximately twice per year. WRF-Chem code can be downloaded at

683   (http://www2.mmm.ucar.edu/wrf/users/download/get_source.html). The corresponding author will

684   provide the bug fixes to version 3.5.1 used in this study, described in Section 2.3, upon request.

Appendix A: Abbreviations and Acronyms

686   DJF: December-January-February (winter)

687   EDGAR: Emission Database for Global Atmospheric Research

688   EEA: European Environmental Agency

689   EOS: Earth Observing System

690   GEOS5: Goddard Earth Observing System Model, Version 5

691   GOCART: Goddard Chemistry Aerosol Radiation and Transport

692   HTAP: Hemispheric Transport of Air Pollution

693   JJA: June-July-August (summer)

694   MADE: Modal Aerosol Dynamics Model for Europe

695   MAM: March-April-May (spring)

696   MERRA: Modern Era-Retrospective Analysis for Research and Applications

697   NCEP: National Centers for Environmental Prediction

698   NCAR: National Center for Atmospheric Research

699   SON: September-October-November (fall)

700   SORGAM: Secondary Organic Aerosol Model

701   WRF-Chem: Weather Research and Forecasting with Chemistry

Appendix B: Definitions of statistical quantities

The statistical quantities used for model evaluation are defined below. Let Obs_i^j and Mod_i^j be the observed and modeled quantities at time i and station j, respectively. N_{obs}^j represents the number of temporal data points evaluated at station j, and N_{obs} represents the total number of data points (each representing a time i and a station j) evaluated in the domain.

The Mean Bias (MB) at a specific station (e.g., Figure 5) is calculated as

$$MB^j = \frac{1}{N_{obs}^j} \sum_{i=1}^{N_{obs}^j} Mod_i^j - Obs_i^j$$

and the domain-wide Mean Bias (e.g., Table 5) as

$$MB = \frac{1}{N_{obs}} \sum_{i,j=1}^{N_{obs}} Mod_i^j - Obs_i^j$$

Domain-wide values for Normalized Mean Bias (NMB) and Mean Fractional Bias (MFB) are calculated analogously.

$$NMB = \frac{\sum_{i=1}^{N_{obs}} Mod_i^j - Obs_i^j}{\sum_{i=1}^{N_{obs}} Obs_i^j}$$

$$MFB = \frac{1}{N_{obs}} \sum_{i,j=1}^{N_{obs}} \frac{Mod_i^j - Obs_i^j}{\frac{Mod_i^j + Obs_i^j}{2}}$$

Temporal correlation between model results and observation is evaluated using the Pearson correlation coefficient (r). The value of r is calculated at each station using

$$r^j = \frac{\sum_{i=1}^{N_{obs}^j} \left(Mod_i^j - \overline{Mod^j}\right)\left(Obs_i^j - \overline{Obs^j}\right)}{\sigma_{mod} \times \sigma_{obs}}$$

Here, the numerator represents the covariance between the model and observations, $\overline{Mod^j}$ and $\overline{Obs^j}$ represent the mean of the model and observations, respectively, and σ is the standard deviation. The domain-wide correlation coefficients (e.g., Table 5) is then calculated as

$$r = \frac{1}{N_j} \sum_{j}^{N_j} r^j$$

where N_j is the total number of stations.

Acknowledgements. The authors would like to thank Renate Forkel for valuable discussions regarding the setup of our WRF-Chem simulation, and two anonymous reviewers for their feedback. The authors also thank Jane Coates for sharing her technique for VOC speciation and valuable discussions regarding chemical mechanisms. We thank TNO for access to the TNO-MACC II emissions inventory, and Hugo Denier van der Gon for helpful discussions regarding emissions. The HTAP v2.2 anthropogenic emissions were obtained from http://edgar.jrc.ec.europa.eu/htap_v2/index.php. The authors thank Christophe Knote and Anna Katinka Petersen for sharing bug fixes for the WRF-Chem MOZART code. WRF-Chem tools for preprocessing boundary conditions as well as biogenic, fire, and anthropogenic emissions were provided by NCAR (http://www.acom.ucar.edu/wrf-chem/download.shtml). Initial and boundary conditions for meteorological fields were obtained from ECMWF, http://www.ecmwf.int/en/research/climate-reanalysis/era-interim. Initial and boundary conditions for chemical fields were from MOZART- 4/GEOS5, provided by NCAR at http://www.acd.ucar.edu/wrf-chem/mozart.shtml. Corine land cover data was obtained from http://www.eea.europa.eu/data-and-maps/data/corine-land-cover-2006-raster-2. We acknowledge the UK Met Office for providing the Global Weather Observation dataset via the British Atmospheric Data Centre. We acknowledge EMEP and the Norwegian Institute for Air Research (NILU) for providing the EMEP chemical observation data via the EBAS database (ebas.nilu.no). AirBase is the public air quality database of the EEA; data were obtained at http://www.eea.europa.eu/data-and-maps/data/airbase-the-european-air-quality-database-7. The WRF-Chem simulations have been performed on the supercomputer HYDRA (http://www.rzg.mpg.de/).

References

Ackermann, I. J., Hass, H., Memmesheimer, M., Ebel, A., Binkowski, F. S., and Shankar, U.: Modal aerosol dynamics model for Europe: development and first applications, Atmospheric Environment, 32, 2981 – 2999, doi:http://dx.doi.org/10.1016/S1352-2310(98)00006-5, http://www.sciencedirect.com/science/article/pii/S1352231098000065, 1998a.

Ackermann, I. J., Hass, H., Memmesheimer, M., Ebel, A., Binkowski, F. S., and Shankar, U.: Modal aerosol dynamics model for Europe: development and first applications, Atmospheric Environment, 32, 2981 – 2999, doi:http://dx.doi.org/10.1016/S1352-2310(98)00006-5, http://www.sciencedirect.com/science/article/pii/S1352231098000065, 1998b.

Akritidis, D., Zanis, P., Katragkou, E., Schultz, M., Tegoulias, I., Poupkou, A., Markakis, K., Pytharoulis, I., and Karacostas, T.: Evaluating the impact of chemical boundary conditions on near surface ozone in regional climate–air quality simulations over Europe, Atmospheric Research, 134, 116 – 130, doi:http://dx.doi.org/10.1016/j.atmosres.2013.07.021, http://www.sciencedirect.com/science/article/pii/S0169809513002135, 2013.

Amann, M., Derwent, D., Forsberg, B., Hänninen, O., Hurley, F., Krzyzanowski, M., de Leeuw, F., Liu, S. J., Mandin, C., Schneider, J., Schwarze, P., and Simpson, D.: Health risks of ozone from long-range transboundary air pollution, Tech. rep., World Health Organization Regional Office for Europe, 2008.

Andersson, E., Kahnert, M., and Devasthale, A.: Methodology for evaluating lateral boundary conditions in the regional chemical transport model MATCH (v5.5.0) using combined satellite and ground-based observations, Geoscientific Model Development, 8, 3747–3763, doi:10.5194/gmd-8-3747-2015, http://www.geosci-model-dev.net/8/3747/2015/, 2015.

Baklanov, A., Schlünzen, K., Suppan, P., Baldasano, J., Brunner, D., Aksoyoglu, S., Carmichael, G., Douros, J., Flemming, J., Forkel, R., Galmarini, S., Gauss, M., Grell, G., Hirtl, M., Joffre, S., Jorba, O., Kaas, E., Kaasik, M., Kallos, G., Kong, X., Korsholm, U., Kurganskiy, A., Kushta, J., Lohmann, U., Mahura, A., Manders-Groot, A., Maurizi, A., Moussiopoulos, N., Rao, S. T., Savage, N., Seigneur, C., Sokhi, R. S., Solazzo, E., Solomos, S., Sørensen, B., Tsegas, G., Vignati, E., Vogel, B., and Zhang, Y.: Online coupled regional meteorology chemistry models in Europe: current status and prospects, Atmospheric Chemistry and Physics, 14, 317–398, doi:10.5194/acp-14-317-2014, http://www.atmos-chem-phys.net/14/317/2014/, 2014.

Beekmann, M. and Vautard, R.: A modelling study of photochemical regimes over Europe: robustness and variability, Atmospheric Chemistry and Physics, 10, 10 067–10 084, doi:10.5194/acp-10-10067-2010, http://www.atmos-chem-phys.net/10/10067/2010/, 2010.

Beljaars, A. C. M.: The parametrization of surface fluxes in large-scale models under free convection, Quarterly Journal of the Royal Meteorological Society, 121, 255–270, doi:10.1002/qj.49712152203, http://dx.doi.org/10.1002/qj.49712152203, 1995.

Bieser, J., Aulinger, A., Matthias, V., Quante, M., and Denier van der Gon, H.: Vertical emission profiles for Europe based on plume rise calculations, Environmental Pollution, 159, 2935–2946, doi:10.1016/j.envpol.2011.04.030, 2011.

Binkowski, F. S. and Shankar, U.: The Regional Particulate Matter Model: 1. Model description and preliminary results, Journal of Geophysical Research: Atmospheres, 100, 26 191–26 209, doi:10.1029/95JD02093, http://dx.doi.org/10.1029/95JD02093, 1995.

Carter, W. P.: A detailed mechanism for the gas-phase atmospheric reactions of organic compounds, Atmospheric Environment. Part A. General Topics, 24, 481 – 518, doi:http://dx.doi.org/10.1016/0960-1686(90)90005-8, http://www.sciencedirect.com/science/article/pii/0960168690900058, 1990.

Chen, F. and Dudhia, J.: Coupling and advanced land surface-hydrology model with the Penn State-NCAR MM5 modeling system, Part I: Model implementation and sensitivity, Mon. Weather Rev., 129, 569–585, 2001.

Chou, M.-D. and Suarez, M. J.: An efficient thermal infrared radiation parametrization for use in general circulation models, NASA Tech. Memo., 104606, 85 pp., 1994.

Coates, J. and Butler, T. M.: A comparison of chemical mechanisms using tagged ozone production potential (TOPP) analysis, Atmospheric Chemistry and Physics, 15, 8795–8808, doi:10.5194/acp-15-8795-2015, http://www.atmos-chem-phys.net/15/8795/2015/, 2015.

Coates, J., Mar, K., Ojha, N., and Butler, T.: The Influence of Temperature on Ozone Production under varying NOx Conditions – a modelling study, Atmospheric Chemistry and Physics Discussions, 2016, 1–18, doi:10.5194/acp-2016-260, http://www.atmos-chem-phys-discuss.net/acp-2016-260/, 2016.

Damian, V., Sandu, A., Damian, M., Potra, F., and Carmichael, G. R.: The kinetic preprocessor KPP-a software environment for solving chemical kinetics, Computers & Chemical Engineering, 26, 1567 – 1579, doi:http://dx.doi.org/10.1016/S0098-1354(02)00128-X, http://www.sciencedirect.com/science/article/pii/S009813540200128X, 2002.

Denier van der Gon, H., Hendriks, C., Kuenen, J., Segers, A., and Visschedijk, A.: Description of current temporal emission patterns and sensitivity of predicted AQ for temporal emission patterns, TNO report, EU FP7 MACC deliverable report D_D-EMIS_1.3, 2011.

EEA: Corine Land Cover 2006 raster data, Copenhagen, Denmark, doi:accessed June 2015, http://www.eea.europa.eu/data-and-maps/data/corine-land-cover-2006-raster-2, 2012.

EEA: Air quality in Europe - 2014 report, Tech. Rep. 5/2014, European Environmental Agency, doi:10.2800/22847, 2014.

Emmons, L. K., Walters, S., Hess, P. G., Lamarque, J.-F., Pfister, G. G., Fillmore, D., Granier, C., Guenther, A., Kinnison, D., Laepple, T., Orlando, J., Tie, X., Tyndall, G., Wiedinmyer, C., Baughcum, S. L., and Kloster, S.: Description and evaluation of the Model for Ozone and Related chemical Tracers, version 4 (MOZART-4), Geoscientific Model Development, 3, 43–67, doi:10.5194/gmd-3-43-2010, http://www.geosci-model-dev.net/3/43/2010/, 2010.

Faraji, M., Kimura, Y., McDonald-Buller, E., and Allen, D.: Comparison of the carbon bond and {SAPRC} photochemical mechanisms under conditions relevant to southeast Texas, Atmospheric Environment, 42, 5821 – 5836, doi:http://dx.doi.org/10.1016/j.atmosenv.2007.07.048, http://www.sciencedirect.com/science/article/pii/S1352231007006565, selected Papers from the First International Conference on Atmospheric Chemical Mechanisms, 2008.

Forkel, R., Werhahn, J., Hansen, A. B., McKeen, S., Peckham, S., Grell, G., and Suppan, P.: Effect of aerosol-radiation feedback on regional air quality – A case study with WRF/Chem, Atmospheric Environment, 53, 202 – 211, doi:http://dx.doi.org/10.1016/j.atmosenv.2011.10.009, http://www.sciencedirect.com/science/article/pii/S1352231011010545, aQMEII: An International Initiative for the Evaluation of Regional-Scale Air Quality Models - Phase 1, 2012.

821 Forkel, R., Balzarini, A., Baró, R., Bianconi, R., Curci, G., Jiménez-Guerrero, P., Hirtl, M., Hon-
822 zak, L., Lorenz, C., Im, U., Pérez, J. L., Pirovano, G., José, R. S., Tuccella, P., Werhahn, J., and
823 Žabkar, R.: Analysis of the WRF-Chem contributions to {AQMEII} phase2 with respect to aerosol
824 radiative feedbacks on meteorology and pollutant distributions, Atmospheric Environment, 115, 630
825 – 645, doi:http://dx.doi.org/10.1016/j.atmosenv.2014.10.056, http://www.sciencedirect.com/science/article/
826 pii/S135223101400853X, 2015.

827 Geiger, H., Barnes, I., Bejan, I., Benter, T., and Spittler, M.: The tropospheric degradation of isoprene: an
828 updated module for the regional atmospheric chemistry mechanism, Atmospheric Environment, 37, 1503 –
829 1519, doi:http://dx.doi.org/10.1016/S1352-2310(02)01047-6, http://www.sciencedirect.com/science/article/
830 pii/S1352231002010476, 2003.

831 Gery, M. W., Whitten, G. Z., Killus, J. P., and Dodge, M. C.: A photochemical kinetics mechanism for urban
832 and regional scale computer modeling, Journal of Geophysical Research: Atmospheres, 94, 12 925–12 956,
833 doi:10.1029/JD094iD10p12925, http://dx.doi.org/10.1029/JD094iD10p12925, 1989.

834 Grell, G. A. and Dévényi, D.: A generalized approach to parameterizing convection combining ensemble and
835 data assimilation techniques, Geophysical Research Letters, 29, 38–1–38–4, doi:10.1029/2002GL015311,
836 http://dx.doi.org/10.1029/2002GL015311, 2002.

837 Grell, G. A., Knoche, R., Peckham, S. E., and McKeen, S. A.: Online versus offline air quality modeling
838 on cloud-resolving scales, Geophysical Research Letters, 31, n/a–n/a, doi:10.1029/2004GL020175, http:
839 //dx.doi.org/10.1029/2004GL020175, l16117, 2004.

840 Grell, G. A., Peckham, S. E., Schmitz, R., McKeen, S. A., Frost, G., Skamarock, W. C., and
841 Eder, B.: Fully coupled "online" chemistry within the WRF model, Atmospheric Environment, 39,
842 doi:10.1016/j.atmosenv.2005.04.027, http://dx.doi.org/10.1016/j.atmosenv.2005.04.027, 2005.

843 Guenther, A., Karl, T., Harley, P., Wiedinmyer, C., Palmer, P. I., and Geron, C.: Estimates of global terrestrial
844 isoprene emissions using MEGAN (Model of Emissions of Gases and Aerosols from Nature), Atmospheric
845 Chemistry and Physics, 6, 3181–3210, doi:10.5194/acp-6-3181-2006, http://www.atmos-chem-phys.net/6/
846 3181/2006/, 2006.

847 Hong, S.-Y., Noh, Y., and Dudhia, J.: A New Vertical Diffusion Package with an Explicit Treatment of Entrain-
848 ment Processes, Monthly Weather Review, 134, 2318–2341, http://dx.doi.org/10.1175/MWR3199.1, doi:
849 10.1175/MWR3199.1, 2006.

850 Iacono, M. J., Delamere, J. S., Mlawer, E. J., Shephard, M. W., Clough, S. A., and Collins, W. D.: Radiative
851 forcing by long-lived greenhouse gases: Calculations with the AER radiative transfer models, Journal of
852 Geophysical Research: Atmospheres, 113, n/a–n/a, doi:10.1029/2008JD009944, http://dx.doi.org/10.1029/
853 2008JD009944, d13103, 2008.

854 Im, U., Bianconi, R., Solazzo, E., Kioutsioukis, I., Badia, A., Balzarini, A., Baró, R., Bellasio, R., Brun-
855 ner, D., Chemel, C., Curci, G., Flemming, J., Forkel, R., Giordano, L., Jiménez-Guerrero, P., Hirtl, M.,
856 Hodzic, A., Honzak, L., Jorba, O., Knote, C., Kuenen, J. J., Makar, P. A., Manders-Groot, A., Neal, L.,
857 Pérez, J. L., Pirovano, G., Pouliot, G., Jose, R. S., Savage, N., Schroder, W., Sokhi, R. S., Syrakov, D.,
858 Torian, A., Tuccella, P., Werhahn, J., Wolke, R., Yahya, K., Zabkar, R., Zhang, Y., Zhang, J., Hogrefe, C.,
859 and Galmarini, S.: Evaluation of operational on-line-coupled regional air quality models over Europe and
860 North America in the context of {AQMEII} phase 2. Part I: Ozone, Atmospheric Environment, 115, 404

861   – 420, doi:http://dx.doi.org/10.1016/j.atmosenv.2014.09.042, http://www.sciencedirect.com/science/article/

862   pii/S1352231014007353, 2015.

863 Janssens-Maenhout, G., Crippa, M., Guizzardi, D., Dentener, F., Muntean, M., Pouliot, G., Keating, T., Zhang,

864   Q., Kurokawa, J., Wankmüller, R., Denier van der Gon, H., Klimont, Z., Frost, G., Darras, S., and Koffi, B.:

865   HTAP v2: a mosaic of regional and global emission gridmaps for 2008 and 2010 to study hemispheric trans-

866   port of air pollution, Atmospheric Chemistry and Physics Discussions, 15, 12 867–12 909, doi:10.5194/acpd-

867   15-12867-2015, http://www.atmos-chem-phys-discuss.net/15/12867/2015/, 2015.

868 Kim, Y., Sartelet, K., and Seigneur, C.: Comparison of two gas-phase chemical kinetic mechanisms of ozone

869   formation over Europe, Journal of Atmospheric Chemistry, 62, 89–119, doi:10.1007/s10874-009-9142-5,

870   http://dx.doi.org/10.1007/s10874-009-9142-5, 2010.

871 Knote, C., Tuccella, P., Curci, G., Emmons, L., Orlando, J. J., Madronich, S., Baró, R., Jiménez-Guerrero,

872   P., Luecken, D., Hogrefe, C., Forkel, R., Werhahn, J., Hirtl, M., Pérez, J. L., José, R. S., Giordano, L.,

873   Brunner, D., Yahya, K., and Zhang, Y.: Influence of the choice of gas-phase mechanism on predictions of

874   key gaseous pollutants during the {AQMEII} phase-2 intercomparison, Atmospheric Environment, 115, 553

875   – 568, doi:http://dx.doi.org/10.1016/j.atmosenv.2014.11.066, http://www.sciencedirect.com/science/article/

876   pii/S1352231014009388, 2015.

877 Kuenen, J., Visschedijk, J., Jozwicka, M., and Denier van der Gon, H.: TNO-MACC_II emission inven-

878   tory: a multi-year (2003-2009) consistent high-resolution European inventory for air quality modelling,

879   Atmospheric Chemistry and Physics, 14, 10 963–10 976, doi:10.5194/acp-14-10963-2014, http://www.

880   atmos-chem-phys.net/14/10963/2014/, 2014.

881 Kuik, F., Lauer, A., Churkina, G., Denier van der Gon, H. A. C., Fenner, D., Mar, K. A., and Butler, T. M.:

882   Air quality modelling in the Berlin-Brandenburg region using WRF-Chem v3.7.1: sensitivity to resolution

883   of model grid and input data, Geoscientific Model Development Discussions, 2016, 1–46, doi:10.5194/gmd-

884   2016-190, http://www.geosci-model-dev-discuss.net/gmd-2016-190/, 2016.

885 Kusaka, H. and Kimura, F.: Thermal Effects of Urban Canyon Structure on the Nocturnal Heat Island: Nu-

886   merical Experiment Using a Mesoscale Model Coupled with an Urban Canopy Model, Journal of Applied

887   Meteorology, 43, 1899–1910, http://dx.doi.org/10.1175/JAM2169.1, doi: 10.1175/JAM2169.1, 2004.

888 Lelieveld, J., Evans, J. S., Fnais, M., Giannadaki, D., and Pozzer, A.: The contribution of outdoor air pol-

889   lution sources to premature mortality on a global scale, Nature, 525, 367–371, http://dx.doi.org/10.1038/

890   nature15371, letter, 2015.

891 Lin, Y.-L., Farley, R. D., and Orville, H. D.: Bulk Parameterization of the Snow Field in a

892   Cloud Model, Journal of Climate and Applied Meteorology, 22, 1065–1092, doi:10.1175/1520-

893   0450(1983)022<1065:BPOTSF>2.0.CO;2, http://dx.doi.org/10.1175/1520-0450(1983)022<1065:

894   BPOTSF>2.0.CO;2, 1983.

895 Liu, P., Tsimpidi, A. P., Hu, Y., Stone, B., Russell, A. G., and Nenes, A.: Differences between downscaling with

896   spectral and grid nudging using WRF, Atmospheric Chemistry and Physics, 12, 3601–3610, doi:10.5194/acp-

897   12-3601-2012, http://www.atmos-chem-phys.net/12/3601/2012/, 2012.

898 Luecken, D., Phillips, S., Sarwar, G., and Jang, C.: Effects of using the {CB05} vs. {SAPRC99} vs. {CB4}

899   chemical mechanism on model predictions: Ozone and gas-phase photochemical precursor concentrations,

900   Atmospheric Environment, 42, 5805 – 5820, doi:http://dx.doi.org/10.1016/j.atmosenv.2007.08.056, http://

901   www.sciencedirect.com/science/article/pii/S1352231007007728, selected Papers from the First International

902   Conference on Atmospheric Chemical Mechanisms, 2008.

903 Mallet, V. and Sportisse, B.: Uncertainty in a chemistry-transport model due to physical parameterizations and

904   numerical approximations: An ensemble approach applied to ozone modeling, Journal of Geophysical Re-

905   search: Atmospheres, 111, n/a–n/a, doi:10.1029/2005JD006149, http://dx.doi.org/10.1029/2005JD006149,

906   d01302, 2006.

907 Mallet, V., Quélo, D., Sportisse, B., Ahmed de Biasi, M., Debry, E., Korsakissok, I., Wu, L., Rous-

908   tan, Y., Sartelet, K., Tombette, M., and Foudhil, H.: Technical Note: The air quality modeling sys-

909   tem Polyphemus, Atmospheric Chemistry and Physics, 7, 5479–5487, doi:10.5194/acp-7-5479-2007, http:

910   //www.atmos-chem-phys.net/7/5479/2007/, 2007.

911 Miguez-Macho, G., Stenchikov, G., and Robock, A.: Spectral nudging to eliminate the effects of domain po-

912   sition and geometry in regional climate model simulations, Journal of Geophysical Research: Atmospheres,

913   109, doi:10.1029/2003JD004495, 2004.

914 Monks, P. S., Archibald, A. T., Colette, A., Cooper, O., Coyle, M., Derwent, R., Fowler, D., Granier, C., Law,

915   K. S., Mills, G. E., Stevenson, D. S., Tarasova, O., Thouret, V., von Schneidemesser, E., Sommariva, R., Wild,

916   O., and Williams, M. L.: Tropospheric ozone and its precursors from the urban to the global scale from air

917   quality to short-lived climate forcer, Atmospheric Chemistry and Physics, 15, 8889–8973, doi:10.5194/acp-

918   15-8889-2015, http://www.atmos-chem-phys.net/15/8889/2015/, 2015.

919 Pfister, G. G., Walters, S., Emmons, L. K., Edwards, D. P., and Avise, J.: Quantifying the contribution

920   of inflow on surface ozone over California during summer 2008, Journal of Geophysical Research:

921   Atmospheres, 118, 12,282–12,299, doi:10.1002/2013JD020336, http://dx.doi.org/10.1002/2013JD020336,

922   2013JD020336, 2013.

923 Sandu, A. and Sander, R.: Technical note: Simulating chemical systems in Fortran90 and Matlab with the

924   Kinetic PreProcessor KPP-2.1, Atmospheric Chemistry and Physics, 6, 187–195, doi:10.5194/acp-6-187-

925   2006, http://www.atmos-chem-phys.net/6/187/2006/, 2006.

926 Schaap, M., Roemer, M., Sauter, F., Boersen, G., Timmermans, R., and Builtjes, P.: LOTOS-EUROS: Docu-

927   mentation, TNO report B&O-A, 2005.

928 Schaap, M., Timmermans, R., Roemer, M., Boersen, G., Builtjes, P., Sauter, F., Velders, G., and Beck,

929   J.: The LOTOS-EUROS model: Description, validation and latest developments, International Journal of

930   Environment and Pollution, 32, 270–290, doi:10.1504/IJEP.2008.017106, http://www.scopus.com/inward/

931   record.url?eid=2-s2.0-39349101242&partnerID=40&md5=af80f203e8a045cbb128dc3b58074135, cited By

932   0, 2008.

933 Schell, B., Ackermann, I. J., Hass, H., Binkowski, F. S., and Ebel, A.: Modeling the formation of secondary

934   organic aerosol within a comprehensive air quality model system, Journal of Geophysical Research: Atmo-

935   spheres, 106, 28 275–28 293, doi:10.1029/2001JD000384, http://dx.doi.org/10.1029/2001JD000384, 2001.

936 Sillman, S.: The use of NO y , H2O2, and HNO3 as indicators for ozone-NO x -hydrocarbon sensitivity in ur-

937   ban locations, Journal of Geophysical Research: Atmospheres, 100, 14 175–14 188, doi:10.1029/94JD02953,

938   http://dx.doi.org/10.1029/94JD02953, 1995.

939 Simpson, D., Benedictow, A., Berge, H., Bergström, R., Emberson, L. D., Fagerli, H., Flechard, C. R.,

940   Hayman, G. D., Gauss, M., Jonson, J. E., Jenkin, M. E., Nyíri, A., Richter, C., Semeena, V. S., Tsyro,

941   S., Tuovinen, J.-P., Valdebenito, A., and Wind, P.: The EMEP MSC-W chemical transport model –tech-

942   nical description, Atmospheric Chemistry and Physics, 12, 7825–7865, doi:10.5194/acp-12-7825-2012,

943   http://www.atmos-chem-phys.net/12/7825/2012/, 2012.

944   Solazzo, E., Bianconi, R., Pirovano, G., Matthias, V., Vautard, R., Moran, M. D., Appel, K. W., Bessagnet,

945   B., Brandt, J., Christensen, J. H., Chemel, C., Coll, I., Ferreira, J., Forkel, R., Francis, X. V., Grell, G.,

946   Grossi, P., Hansen, A. B., Miranda, A. I., Nopmongcol, U., Prank, M., Sartelet, K. N., Schaap, M., Silver,

947   J. D., Sokhi, R. S., Vira, J., Werhahn, J., Wolke, R., Yarwood, G., Zhang, J., Rao, S. T., and Galmarini,

948   S.: Operational model evaluation for particulate matter in Europe and North America in the context of

949   {AQMEII}, Atmospheric Environment, 53, 75 – 92, doi:http://dx.doi.org/10.1016/j.atmosenv.2012.02.045,

950   http://www.sciencedirect.com/science/article/pii/S1352231012001604, aQMEII: An International Initiative

951   for the Evaluation of Regional-Scale Air Quality Models - Phase 1, 2012a.

952   Solazzo, E., Bianconi, R., Vautard, R., Appel, K. W., Moran, M. D., Hogrefe, C., Bessagnet, B., Brandt, J.,

953   Christensen, J. H., Chemel, C., Coll, I., van der Gon, H. D., Ferreira, J., Forkel, R., Francis, X. V., Grell,

954   G., Grossi, P., Hansen, A. B., Jeričević, A., Kraljević, L., Miranda, A. I., Nopmongcol, U., Pirovano, G.,

955   Prank, M., Riccio, A., Sartelet, K. N., Schaap, M., Silver, J. D., Sokhi, R. S., Vira, J., Werhahn, J., Wolke, R.,

956   Yarwood, G., Zhang, J., Rao, S., and Galmarini, S.: Model evaluation and ensemble modelling of surface-

957   level ozone in Europe and North America in the context of {AQMEII}, Atmospheric Environment, 53, 60 –

958   74, doi:http://dx.doi.org/10.1016/j.atmosenv.2012.01.003, http://www.sciencedirect.com/science/article/pii/

959   S1352231012000064, aQMEII: An International Initiative for the Evaluation of Regional-Scale Air Quality

960   Models - Phase 1, 2012b.

961   Stauffer, D. R., Seaman, N. L., and Binkowski, F. S.: Use of Four-Dimensional Data Assimilation in a Limited-

962   Area Mesoscale Model Part II: Effects of Data Assimilation within the Planetary Boundary Layer, Mon.

963   Wea. Rev., 119, 734–754, doi:10.1175/1520-0493(1991)119<0734:UOFDDA>2.0.CO;2, http://dx.doi.org/

964   10.1175/1520-0493(1991)119<0734:UOFDDA>2.0.CO;2, 1991.

965   Stegehuis, A., Vautard, R., Ciais, P., Teuling, A., Miralles, D., and Wild., M.: An observation-constrained multi-

966   physics RCM ensemble for simulating European mega-heatwaves, Geoscientific Model Development Dis-

967   cussions, 7, 7861–7886, doi:10.5194/gmdd-7-7861-2014, 2014.

968   Stevenson, D. S., Young, P. J., Naik, V., Lamarque, J.-F., Shindell, D. T., Voulgarakis, A., Skeie, R. B., Dal-

969   soren, S. B., Myhre, G., Berntsen, T. K., Folberth, G. A., Rumbold, S. T., Collins, W. J., MacKenzie, I. A.,

970   Doherty, R. M., Zeng, G., van Noije, T. P. C., Strunk, A., Bergmann, D., Cameron-Smith, P., Plummer, D. A.,

971   Strode, S. A., Horowitz, L., Lee, Y. H., Szopa, S., Sudo, K., Nagashima, T., Josse, B., Cionni, I., Righi, M.,

972   Eyring, V., Conley, A., Bowman, K. W., Wild, O., and Archibald, A.: Tropospheric ozone changes, radia-

973   tive forcing and attribution to emissions in the Atmospheric Chemistry and Climate Model Intercomparison

974   Project (ACCMIP), Atmospheric Chemistry and Physics, 13, 3063–3085, doi:10.5194/acp-13-3063-2013,

975   http://www.atmos-chem-phys.net/13/3063/2013/, 2013.

976   Stockwell, W. R., Middleton, P., Chang, J. S., and Tang, X.: The second generation regional acid deposition

977   model chemical mechanism for regional air quality modeling, Journal of Geophysical Research: Atmo-

978   spheres, 95, 16 343–16 367, doi:10.1029/JD095iD10p16343, http://dx.doi.org/10.1029/JD095iD10p16343,

979   1990.

980 Stockwell, W. R., Kirchner, F., Kuhn, M., and Seefeld, S.: A new mechanism for regional atmospheric chemistry

981 modeling, Journal of Geophysical Research: Atmospheres, 102, 25 847–25 879, doi:10.1029/97JD00849,

982 http://dx.doi.org/10.1029/97JD00849, 1997.

983 Terrenoire, E., Bessagnet, B., Rouïl, L., Tognet, F., Pirovano, G., Létinois, L., Beauchamp, M., Colette, A.,

984 Thunis, P., Amann, M., and Menut, L.: High-resolution air quality simulation over Europe with the chemistry

985 transport model CHIMERE, Geoscientific Model Development, 8, 21–42, doi:10.5194/gmd-8-21-2015, http:

986 //www.geosci-model-dev.net/8/21/2015/, 2015.

987 Tørseth, K., Aas, W., Breivik, K., Fjæraa, A. M., Fiebig, M., Hjellbrekke, A. G., Lund Myhre, C., Solberg, S.,

988 and Yttri, K. E.: Introduction to the European Monitoring and Evaluation Programme (EMEP) and observed

989 atmospheric composition change during 1972–2009, Atmospheric Chemistry and Physics, 12, 5447–5481,

990 doi:10.5194/acp-12-5447-2012, http://www.atmos-chem-phys.net/12/5447/2012/, 2012.

991 Tuccella, P., Curci, G., Visconti, G., Bessagnet, B., Menut, L., and Park, R. J.: Modeling of gas and aerosol with

992 WRF/Chem over Europe: Evaluation and sensitivity study, Journal of Geophysical Research: Atmospheres,

993 117, n/a–n/a, doi:10.1029/2011JD016302, http://dx.doi.org/10.1029/2011JD016302, d03303, 2012.

994 von Schneidemesser, E., Coates, J., van der Gon, H. D., Visschedijk, A., and Butler, T.: Variation of the

995 {NMVOC} speciation in the solvent sector and the sensitivity of modelled tropospheric ozone, Atmospheric

996 Environment, 135, 59 – 72, doi:http://dx.doi.org/10.1016/j.atmosenv.2016.03.057, http://www.sciencedirect.

997 com/science/article/pii/S1352231016302242, 2016.

998 Žabkar, R., Honzak, L., Skok, G., Forkel, R., Rakovec, J., Ceglar, A., and Žagar, N.: Evaluation of the high reso-

999 lution WRF-Chem (v3.4.1) air quality forecast and its comparison with statistical ozone predictions, Geosci-

1000 entific Model Development, 8, 2119–2137, doi:10.5194/gmd-8-2119-2015, http://www.geosci-model-dev.

1001 net/8/2119/2015/, 2015.

1002 Wang, W., Bruyère, C., Duda, M., Dudhia, J., Gill, D., Kavulich, M., Keene, K., Lin, H.-C., Michalakes, J.,

1003 Rizvi, S., and Zhang, X.: ARW Version 3 Modeling System User's Guide, Chapter 3: WRF Preprocessing

1004 System (WPS), pp. 59–60, 2014.

1005 WHO: Health Aspects of Air Pollution with Particulate Matter, Ozone and Nitrogen Dioxide, Bonn, 2003.

1006 WHO, R. O. f. E.: Review of evidence on health aspects of air pollution – REVIHAAP Project, Tech. rep.,

1007 World Health Organization, 2013.

1008 Wiedinmyer, C., Akagi, S. K., Yokelson, R. J., Emmons, L. K., Al-Saadi, J. A., Orlando, J. J., and Soja, A. J.:

1009 The Fire INventory from NCAR (FINN): a high resolution global model to estimate the emissions from

1010 open burning, Geoscientific Model Development, 4, 625–641, doi:10.5194/gmd-4-625-2011, http://www.

1011 geosci-model-dev.net/4/625/2011/, 2011.

1012 Wilson, R. C., Fleming, Z. L., Monks, P. S., Clain, G., Henne, S., Konovalov, I. B., Szopa, S., and Menut, L.:

1013 Have primary emission reduction measures reduced ozone across Europe? An analysis of European rural

1014 background ozone trends 1996–2005, Atmospheric Chemistry and Physics, 12, 437–454, doi:10.5194/acp-

1015 12-437-2012, http://www.atmos-chem-phys.net/12/437/2012/, 2012.

1016 Yarwood, G., Stoeckenius, T. E., Heiken, J. G., and Dunker, A. M.: Modeling Weekday/Weekend Ozone Dif-

1017 ferences in the Los Angeles Region for 1997, Journal of the Air & Waste Management Association, 53, 864–

1018 875, doi:10.1080/10473289.2003.10466232, http://dx.doi.org/10.1080/10473289.2003.10466232, 2003.

1019 Yarwood, G., Rao, S., Yocke, M., and Whitten, G. Z.: Updates to the Carbon Bond Chemical Mechanism:
1020   CB05, Tech. rep., U. S Environmental Protection Agency, 2005.

1021 Zaveri, R. A. and Peters, L. K.: A new lumped structure photochemical mechanism for large-scale applications,
1022   Journal of Geophysical Research: Atmospheres, 104, 30 387–30 415, doi:10.1029/1999JD900876, http://dx.
1023   doi.org/10.1029/1999JD900876, 1999.

1024 Zhang, Y.: Online-coupled meteorology and chemistry models: history, current status, and outlook, Atmo-
1025   spheric Chemistry and Physics, 8, 2895–2932, doi:10.5194/acp-8-2895-2008, http://www.atmos-chem-phys.
1026   net/8/2895/2008/, 2008.

1027 Zhang, Y., Pan, Y., Wang, K., Fast, J. D., and Grell, G. A.: WRF/Chem-MADRID: Incorporation of an aerosol
1028   module into WRF/Chem and its initial application to the TexAQS2000 episode, Journal of Geophysical Re-
1029   search: Atmospheres, 115, n/a–n/a, doi:10.1029/2009JD013443, http://dx.doi.org/10.1029/2009JD013443,
1030   d18202, 2010.

1031 Zhang, Y., Chen, Y., Sarwar, G., and Schere, K.: Impact of gas-phase mechanisms on Weather Research
1032   Forecasting Model with Chemistry (WRF/Chem) predictions: Mechanism implementation and compara-
1033   tive evaluation, Journal of Geophysical Research: Atmospheres, 117, n/a–n/a, doi:10.1029/2011JD015775,
1034   http://dx.doi.org/10.1029/2011JD015775, d01301, 2012.

1035 Zhang, Y., Sartelet, K., Wu, S.-Y., and Seigneur, C.: Application of WRFChem-MADRID and WRFPolyphemus
1036   in Europe – Part 1: Model description, evaluation of meteorological predictions, and aerosol–meteorology
1037   interactions, Atmospheric Chemistry and Physics, 13, 6807–6843, doi:10.5194/acp-13-6807-2013, http://
1038   www.atmos-chem-phys.net/13/6807/2013/, 2013a.

1039 Zhang, Y., Sartelet, K., Zhu, S., Wang, W., Wu, S.-Y., Zhang, X., Wang, K., Tran, P., Seigneur, C., and
1040   Wang, Z.-F.: Application of WRF/Chem-MADRID and WRF/Polyphemus in Europe – Part 2: Evaluation of
1041   chemical concentrations and sensitivity simulations, Atmospheric Chemistry and Physics, 13, 6845–6875,
1042   doi:10.5194/acp-13-6845-2013, http://www.atmos-chem-phys.net/13/6845/2013/, 2013b.

Table 1. WRF-Chem options used in model simulations.

Atmospheric Process	Option used
Cloud microphysics	Lin et al. scheme (Lin et al., 1983)
Longwave radiation	RRTMG (Iacono et al., 2008)
Shortwave radiation	Goddard shortwave scheme (Chou and Suarez, 1994)
Surface Layer	MM5 Similarity based on Monin-Obukhov scheme (Beljaars, 1995)
Land-surface Physics	Noah Land Surface Model (Chen and Dudhia, 2001)
Urban surface physics	Urban Canopy Model (Kusaka and Kimura, 2004)
Planetary boundary layer	Yonsei University scheme (Hong et al., 2006)
Cumulus parametrization	Grell 3D scheme (Grell and Dévényi, 2002)

Table 2. Description of WRF-Chem simulations performed for this study.

	Simulation Name	Model Chemistry	Photolysis Scheme
(1)	MOZART	MOZART- 4 chemistry with gocart aerosols, KPP solver	Madronich F-TUV photolysis
(2)	RADM2	RADM2 chemistry with MADE/SORGAM aerosols, KPP solver	Madronich photolysis (TUV)

Table 3. Observational datasets used for model evaluation.

Database	Parameter	Temporal Resolution	Data Source
BADC Global Weather Observation Data	MSLP, T2, WS10, WD10	3-hourly	http://badc.nerc.ac.uk/home/
AirBase v7	O_3, NO_2, NO, NO_x	hourly	http://www.eea.europa.eu/data-and-maps/data/airbase-the-european-air-quality-database-7
EMEP	NO_2, NO, NO_x	hourly	http://ebas.nilu.no/

Table 4. Domain-wide statistical performance of WRF-Chem against 3-hourly meteorological observations from BADC. Modeled quantities are from the MOZART simulation.

	Winter (DJF)							Spring (MAM)						
	Mean-Obs	Mean-Mod	MB	NMB	MFB	r	no. stations	Mean-Obs	Mean-Mod	MB	NMB	MFB	r	no. stations
MSLP (hPa)	1015.41	1014.79	-0.96	0.00	0.00	0.99	1297	1014.67	1014.46	-0.35	0.00	0.00	0.99	1295
T2 (° C)	2.51	2.99	0.29	0.11	-0.01	0.89	1581	9.73	9.91	-0.11	-0.01	0.07	0.94	1581
WS10 (m/s)	4.31	5.60	1.34	0.31	0.42	0.71	1577	3.86	4.46	0.65	0.17	0.29	0.68	1589
WD10 (deg)	175.53	203.73	27.93	0.16	0.27	0.50	1568	167.88	188.67	21.16	0.13	0.25	0.48	1580

	Summer (JJA)							Fall (SON)						
	Mean-Obs	Mean-Mod	MB	NMB	MFB	r	no. stations	Mean-Obs	Mean-Mod	MB	NMB	MFB	r	no. stations
MSLP (hPa)	1012.12	1012.11	0.04	0.00	0.00	0.98	1288	1017.61	1017.42	-0.49	0.00	0.00	0.99	1297
T2 (° C)	17.82	17.70	-0.38	-0.02	0.00	0.87	1573	9.20	9.65	0.24	0.03	-0.08	0.95	1583
WS10 (m/s)	3.45	3.90	0.48	0.14	0.27	0.63	1574	3.64	4.61	1.04	0.28	0.40	0.68	1585
WD10 (deg)	173.88	196.92	23.27	0.13	0.25	0.45	1561	172.30	196.49	24.02	0.14	0.27	0.48	1574

Table 5. Statistics for MOZART simulation against hourly observations from the AirBase network. Means and MB are expressed in $\mu g\,m^{-3}$; NMB, MFB, and r are unitless. r is the hourly temporal correlation coefficient for all quantities except MDA8, for which it represents the daily temporal correlation coefficient.

	Winter (DJF)							Spring (MAM)						
	Mean-Obs	Mean-Mod	MB	NMB	MFB	r	no. sta-tions	Mean-Obs	Mean-Mod	MB	NMB	MFB	r	no. sta-tions
O$_3$	53.82	48.34	-5.44	-0.10	-0.10	0.60	366	75.26	70.93	-4.25	-0.06	-0.07	0.56	371
MDA8	67.50	64.20	-3.30	-0.05	-0.04	0.76	365	96.33	97.00	0.67	0.01	0.00	0.69	370
NO$_x$	20.22	16.99	-3.20	-0.16	0.00	0.37	204	14.30	13.32	-0.99	-0.07	-0.15	0.25	210
NO$_2$	14.40	14.83	0.48	0.03	0.07	0.42	250	11.34	12.03	0.70	0.06	-0.10	0.30	252
NO	4.27	1.18	-3.10	-0.73	-1.24	0.29	148	2.65	0.79	-1.87	-0.70	-1.26	0.27	148

	Summer (JJA)							Fall (SON)						
	Mean-Obs	Mean-Mod	MB	NMB	MFB	r	no. sta-tions	Mean-Obs	Mean-Mod	MB	NMB	MFB	r	no. sta-tions
O$_3$	70.84	80.72	9.92	0.14	0.14	0.55	370	47.24	53.10	6.14	0.13	0.13	0.57	367
MDA8	94.51	110.37	15.86	0.17	0.16	0.61	369	63.81	74.82	11.01	0.17	0.15	0.65	367
NO$_x$	10.63	10.57	-0.10	-0.01	-0.21	0.16	206	19.14	16.62	-2.53	-0.13	-0.07	0.32	208
NO$_2$	8.30	9.66	1.37	0.17	-0.12	0.22	248	13.60	15.23	1.64	0.12	0.05	0.38	253
NO	2.01	0.48	-1.53	-0.76	-1.36	0.19	148	4.24	1.07	-3.17	-0.75	-1.32	0.28	146

Table 6. Statistics for MOZART simulation against hourly observations from the EMEP network. Means and MB are expressed in $\mu g\,m^{-3}$; NMB, MFB, and r are unitless. r is the hourly temporal correlation coefficient for all quantities except MDA8, for which it represents the daily temporal correlation coefficient.

	Winter (DJF)							Spring (MAM)						
	Mean-Obs	Mean-Mod	MB	NMB	MFB	r	no. sta-tions	Mean-Obs	Mean-Mod	MB	NMB	MFB	r	no. sta-tions
O$_3$	54.54	43.82	-10.46	-0.19	-0.22	0.53	118	78.99	68.62	-10.53	-0.13	-0.16	0.55	120
MDA8	64.66	55.09	-9.57	-0.15	-0.16	0.56	117	95.64	90.15	-5.49	-0.06	-0.07	0.65	119
NO$_x$	11.36	12.39	1.10	0.10	0.18	0.42	8	10.21	10.44	0.41	0.04	-0.04	0.33	9
NO$_2$	10.19	13.24	3.09	0.30	0.25	0.53	34	8.07	10.72	2.55	0.32	-0.01	0.37	38
NO	2.10	1.22	-0.87	-0.41	-0.65	0.36	25	1.34	0.78	-0.56	-0.42	-0.50	0.35	27

	Summer (JJA)							Fall (SON)						
	Mean-Obs	Mean-Mod	MB	NMB	MFB	r	no. sta-tions	Mean-Obs	Mean-Mod	MB	NMB	MFB	r	no. sta-tions
O$_3$	72.08	76.39	4.04	0.06	0.06	0.54	120	53.24	52.05	-1.08	-0.02	-0.02	0.54	122
MDA8	91.24	101.48	10.24	0.11	0.11	0.59	119	66.99	70.37	3.39	0.05	0.04	0.57	121
NO$_x$	7.62	8.44	0.94	0.12	-0.12	0.30	9	11.83	12.14	0.76	0.06	0.03	0.34	9
NO$_2$	6.07	9.10	2.96	0.49	0.06	0.30	38	8.88	13.81	5.08	0.57	0.23	0.40	38
NO	1.23	0.60	-0.64	-0.52	-0.52	0.28	29	1.42	1.23	-0.14	-0.10	-0.36	0.34	28

Table 7. Statistics for yearly SOMO35 in $mg\,m^{-3} \cdot days$.

Simulation	Observation network	Obs	Model	MB	NMB	MFB	no. stations
MOZART	AirBase	6.23	8.22	1.98	0.32	0.30	375
MOZART	EMEP	5.73	6.27	0.51	0.09	0.11	122
RADM2	AirBase	6.23	2.55	-3.68	-0.59	-0.87	375
RADM2	EMEP	5.73	1.84	-3.91	-0.68	-1.13	122

Table 8. Statistics for RADM2 simulation against hourly observations from the AirBase network. Means and MB are expressed in $\mu g\,m^{-3}$; NMB, MFB, and r are unitless. r is the hourly temporal correlation coefficient for all quantities except MDA8, for which it represents the daily temporal correlation coefficient.

	Winter (DJF)							Spring (MAM)						
	Mean-Obs	Mean-Mod	MB	NMB	MFB	r	no. stations	Mean-Obs	Mean-Mod	MB	NMB	MFB	r	no. stations
O$_3$	53.82	41.57	-12.18	-0.23	-0.25	0.60	366	75.26	53.36	-21.81	-0.29	-0.33	0.53	371
MDA8	67.50	56.04	-11.46	-0.17	-0.17	0.75	365	96.33	74.73	-21.60	-0.22	-0.25	0.67	370
NO$_x$	20.22	13.75	-6.45	-0.32	-0.23	0.36	204	14.30	11.44	-2.87	-0.20	-0.32	0.21	210
NO$_2$	14.40	11.90	-2.47	-0.17	-0.15	0.41	250	11.34	10.31	-1.01	-0.09	-0.27	0.27	252
NO	4.27	0.97	-3.31	-0.77	-1.34	0.27	148	2.65	0.67	-1.99	-0.75	-1.34	0.26	148
	Summer (JJA)							Fall (SON)						
	Mean-Obs	Mean-Mod	MB	NMB	MFB	r	no. stations	Mean-Obs	Mean-Mod	MB	NMB	MFB	r	no. stations
O$_3$	70.84	57.79	-13.01	-0.18	-0.18	0.58	370	47.24	39.00	-8.03	-0.17	-0.18	0.59	367
MDA8	94.51	80.59	-13.92	-0.15	-0.15	0.71	369	63.81	56.02	-7.79	-0.12	-0.12	0.69	367
NO$_x$	10.63	9.79	-0.87	-0.08	-0.29	0.14	206	19.14	14.30	-4.84	-0.25	-0.24	0.30	208
NO$_2$	8.30	8.95	0.67	0.08	-0.19	0.21	248	13.60	12.57	-1.01	-0.07	-0.13	0.36	253
NO	2.01	0.46	-1.55	-0.77	-1.42	0.18	148	4.24	1.28	-2.97	-0.70	-1.27	0.26	146

Table 9. Statistics for RADM2 simulation against hourly observations from the EMEP network. Means and MB are expressed in $\mu g\,m^{-3}$; NMB, MFB, and r are unitless. r is the hourly temporal correlation coefficient for all quantities except MDA8, for which it represents the daily temporal correlation coefficient.

	Winter (DJF)							Spring (MAM)						
	Mean-Obs	Mean-Mod	MB	NMB	MFB	r	no. sta-tions	Mean-Obs	Mean-Mod	MB	NMB	MFB	r	no. sta-tions
O$_3$	54.54	38.67	-15.62	-0.29	-0.36	0.54	118	78.99	53.24	-25.83	-0.33	-0.40	0.49	120
MDA8	64.66	49.40	-15.26	-0.24	-0.27	0.56	117	95.64	71.04	-24.60	-0.26	-0.29	0.55	119
NO$_x$	11.36	10.31	-0.99	-0.09	-0.02	0.38	8	10.21	8.76	-1.31	-0.13	-0.24	0.30	9
NO$_2$	10.19	10.72	0.56	0.06	0.03	0.51	34	8.07	9.11	0.95	0.12	-0.19	0.34	38
NO	2.10	1.16	-0.93	-0.44	-0.67	0.37	25	1.34	0.68	-0.67	-0.50	-0.59	0.31	27

	Summer (JJA)							Fall (SON)						
	Mean-Obs	Mean-Mod	MB	NMB	MFB	r	no. sta-tions	Mean-Obs	Mean-Mod	MB	NMB	MFB	r	no. sta-tions
O$_3$	72.08	55.65	-16.65	-0.23	-0.24	0.58	120	53.24	39.89	-13.21	-0.25	-0.29	0.57	122
MDA8	91.24	74.75	-16.49	-0.18	-0.19	0.69	119	66.99	54.31	-12.68	-0.19	-0.21	0.63	121
NO$_x$	7.62	7.61	0.10	0.01	-0.24	0.28	9	11.83	10.59	-0.82	-0.07	-0.13	0.32	9
NO$_2$	6.07	8.33	2.20	0.36	-0.02	0.29	38	8.88	11.48	2.71	0.31	0.04	0.39	38
NO	1.23	0.52	-0.73	-0.59	-0.58	0.25	29	1.42	1.43	0.07	0.05	-0.31	0.31	28
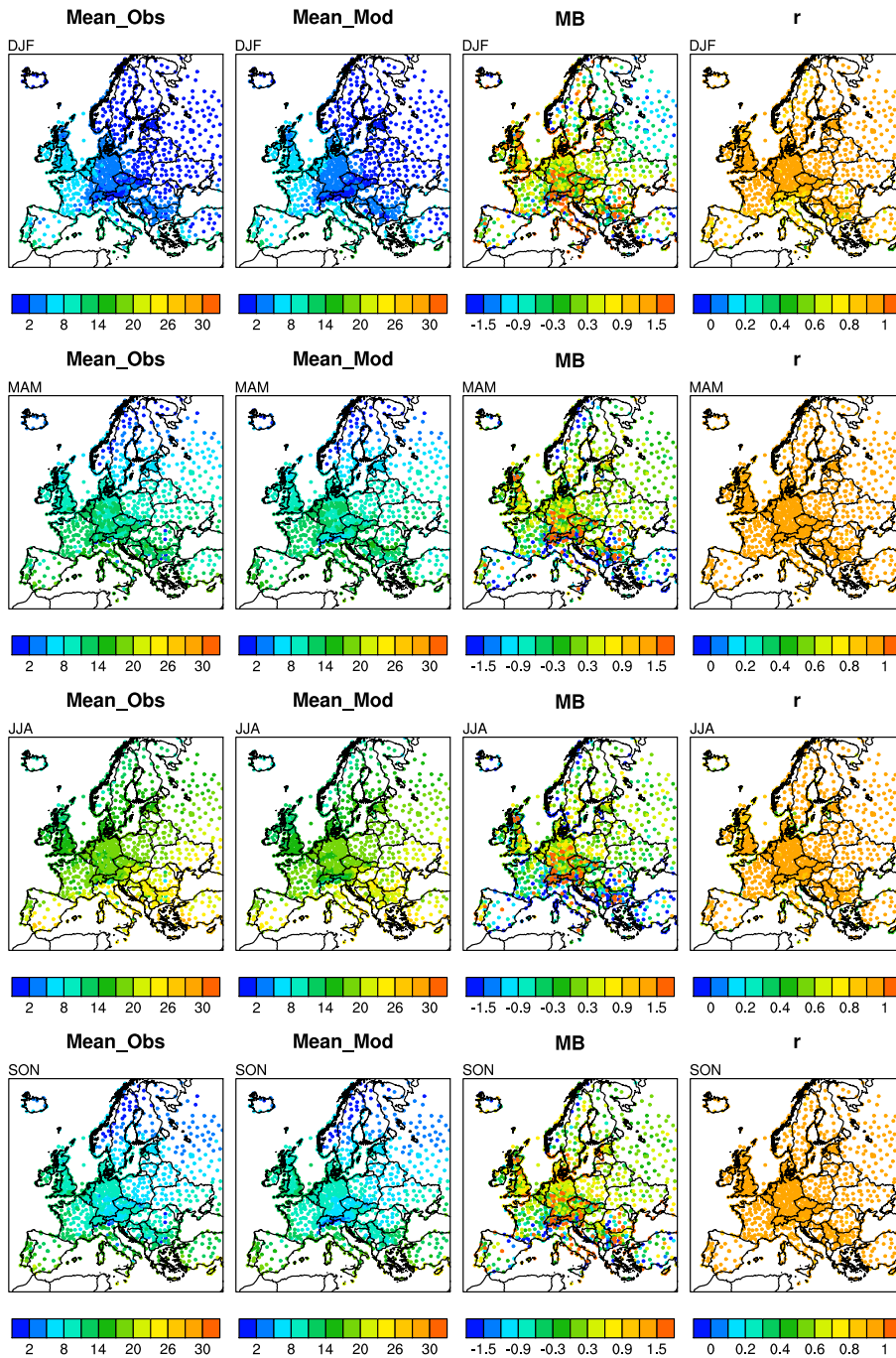
Figure 1. Seasonal average values of 2-meter temperature (T2) in degrees Celcius. Model results and statistics are shown for the MOZART simulation at the locations of the observations.
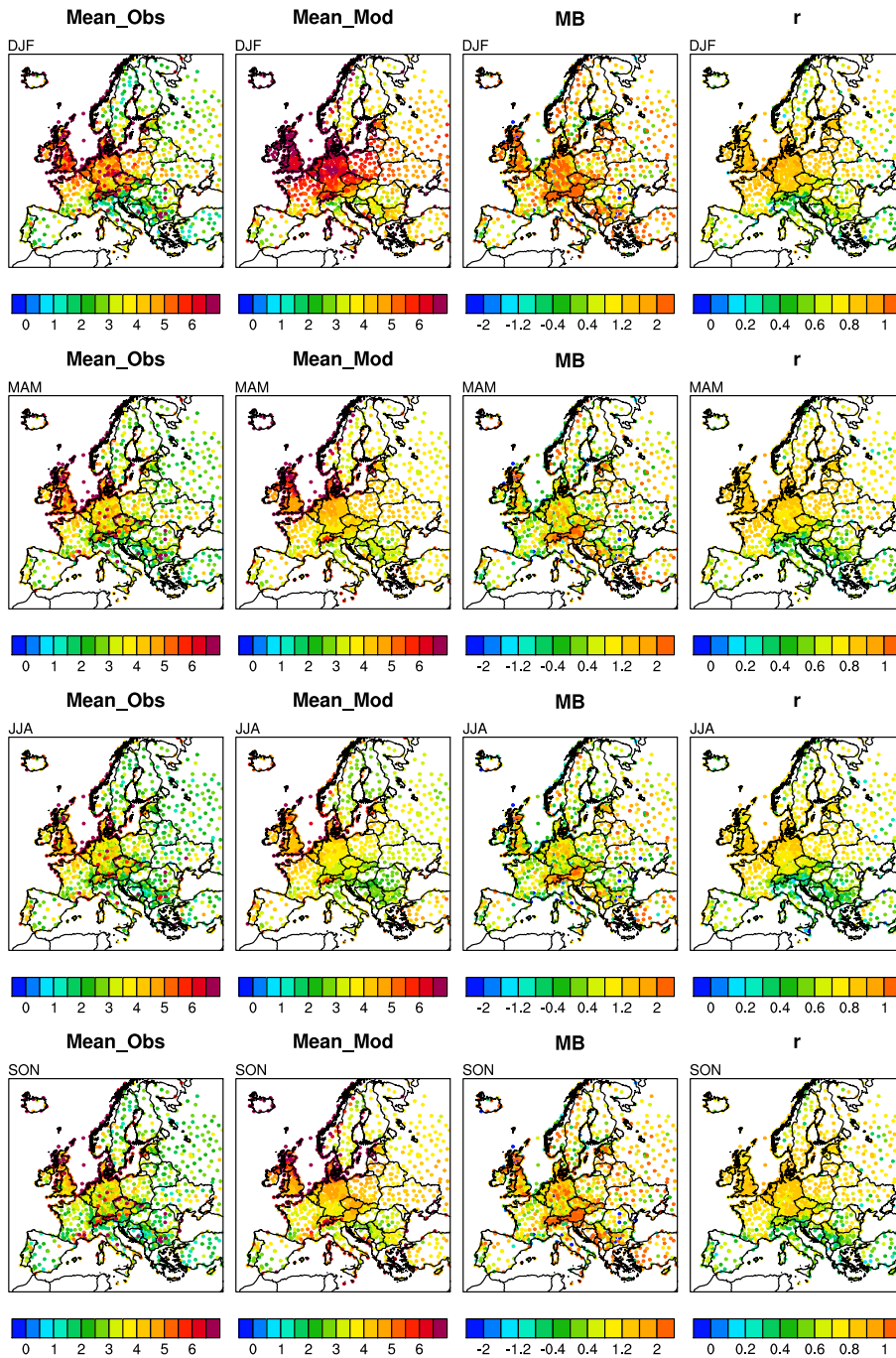
Figure 2. Seasonal average values of 10-meter wind speed (WS10) in m/s. Model results and statistics are shown for the MOZART simulation at the locations of the observations.
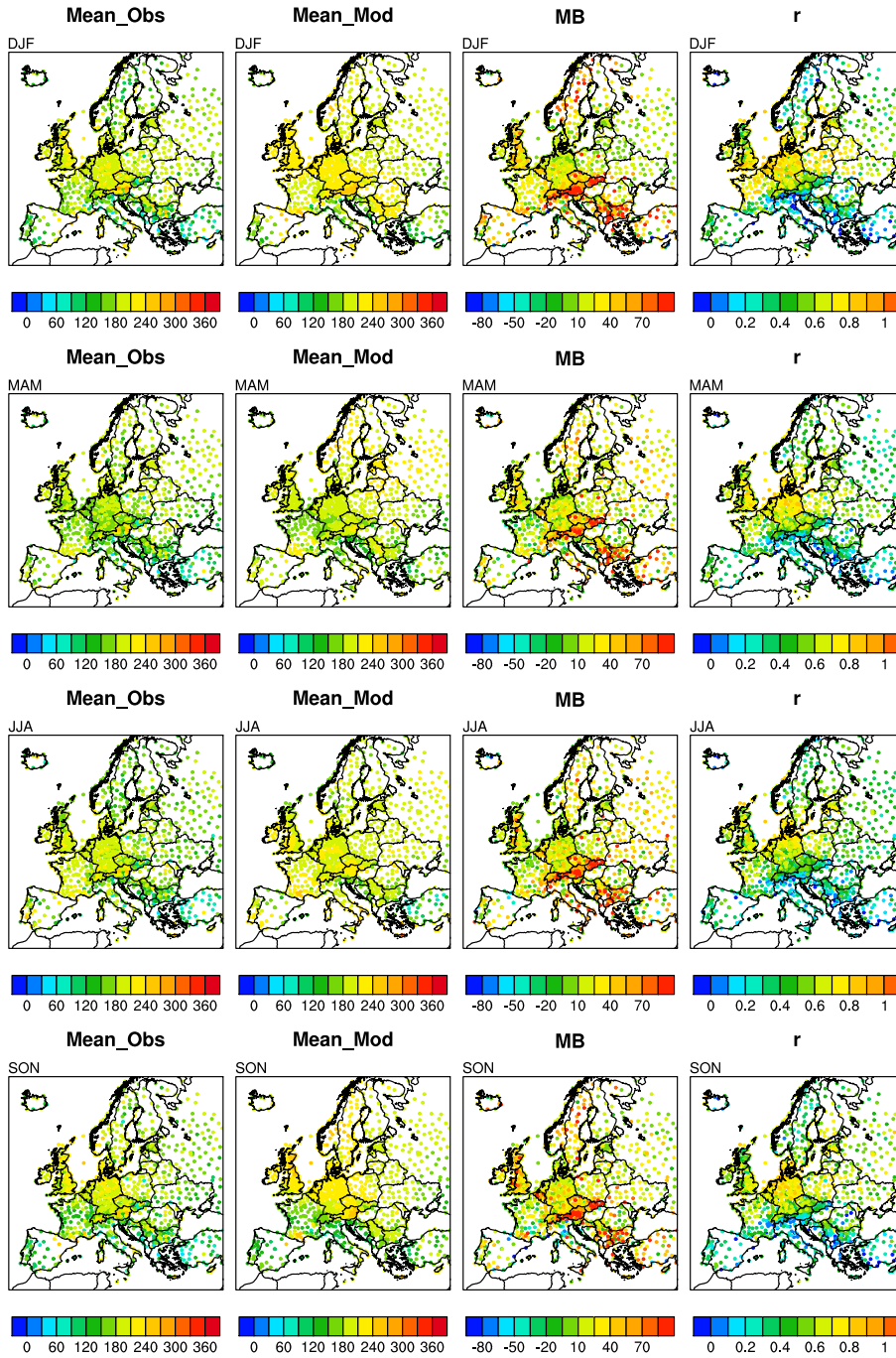
Figure 3. Seasonal average values of 10-meter wind direction (WD10) in degrees. Model results and statistics are shown for the MOZART simulation at the locations of the observations.
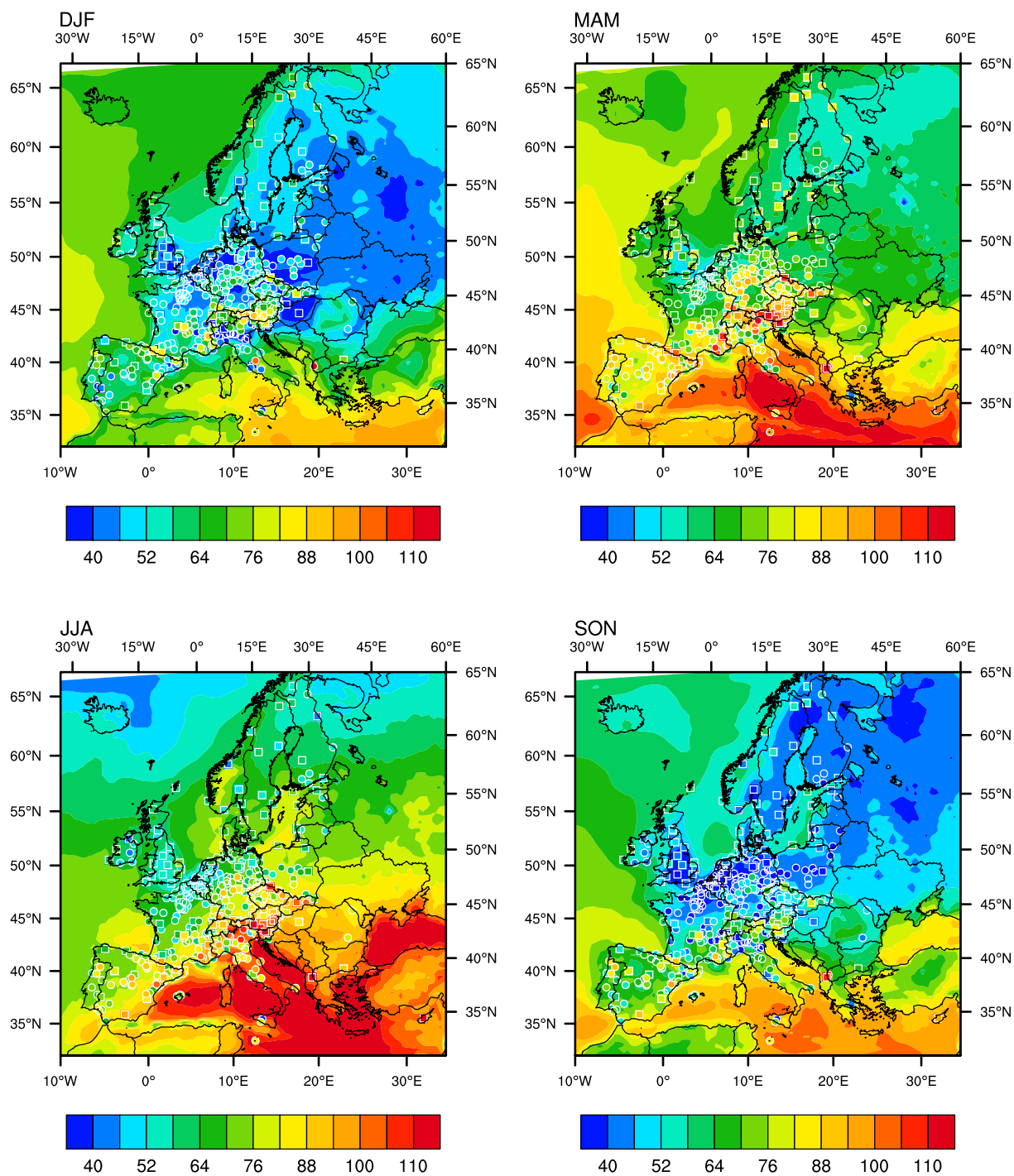
Figure 4. Seasonal average values of surface O_3 in µg m^{-3}. Contours are model output from the MOZART simulation. Filled dots represent hourly measurements at AirBase rural background stations, filled squares represent measurements at EMEP stations.
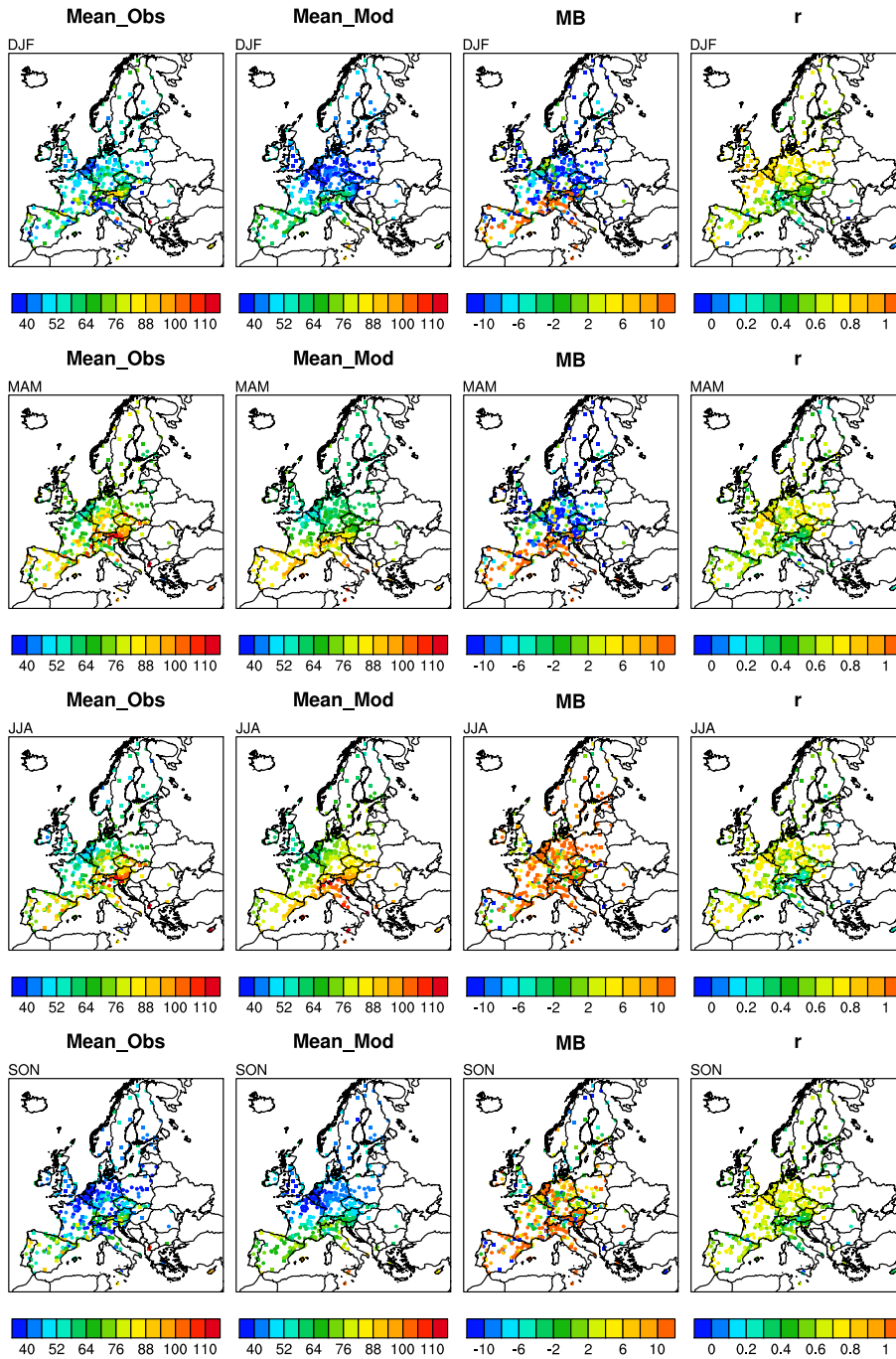
Figure 5. Seasonal average values of surface O_3 in $\mu g\,m^{-3}$ from hourly measurements at AirBase (circles) and EMEP (squares) stations, and modeled values from MOZART for corresponding locations. The Mean Bias (MB, in $\mu g\,m^{-3}$) and temporal correlation coefficient (r) for hourly values are also shown at the location of station observations.
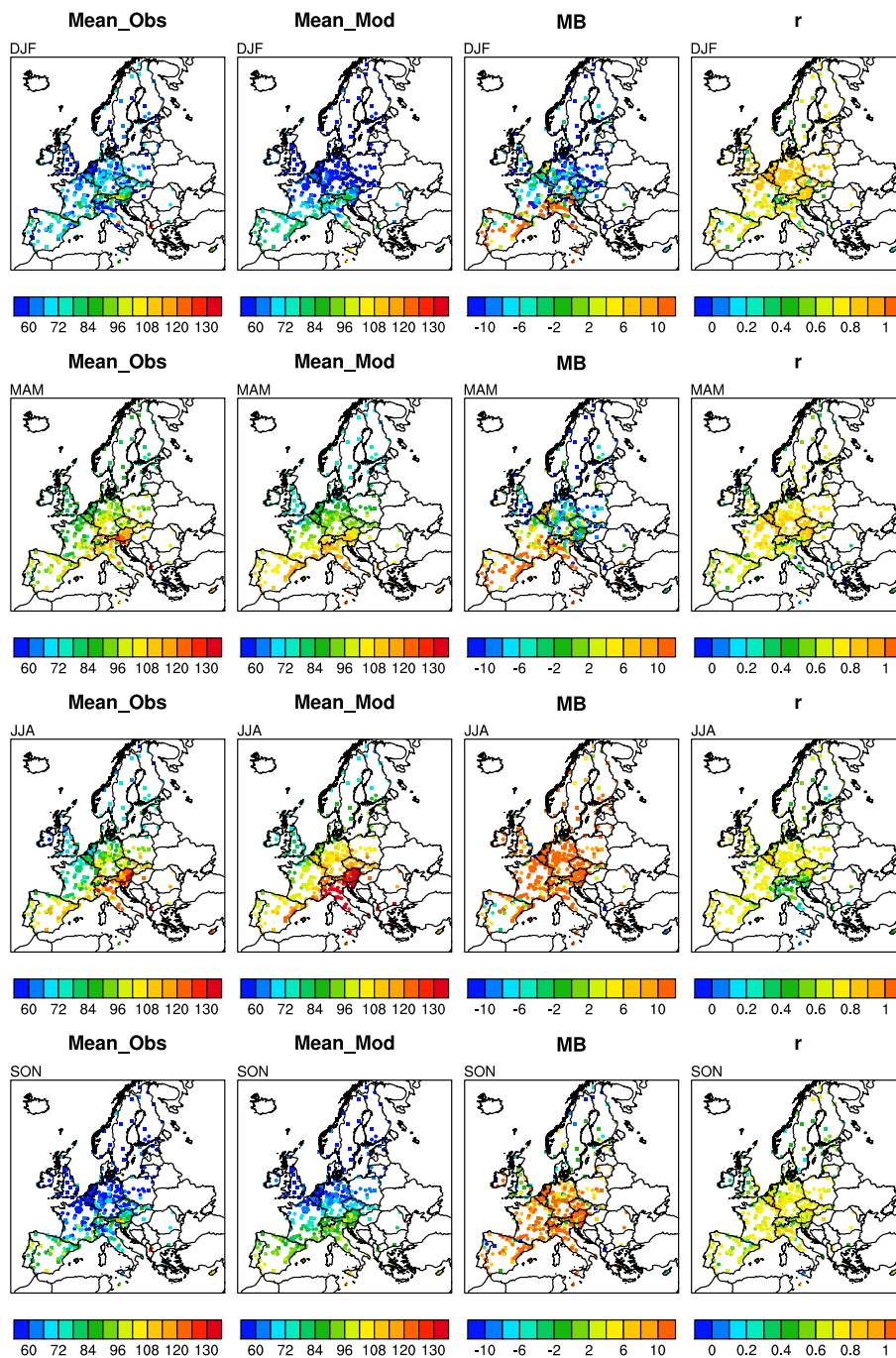
Figure 6. Seasonal average values of MDA8 in µg m^{-3} calculated from hourly measurements at AirBase (circles) and EMEP (squares) stations, and modeled values from MOZART for corresponding locations. The Mean Bias (MB, in µg m^{-3}) and temporal correlation coefficient (r) for daily values are also shown at the location of station observations.
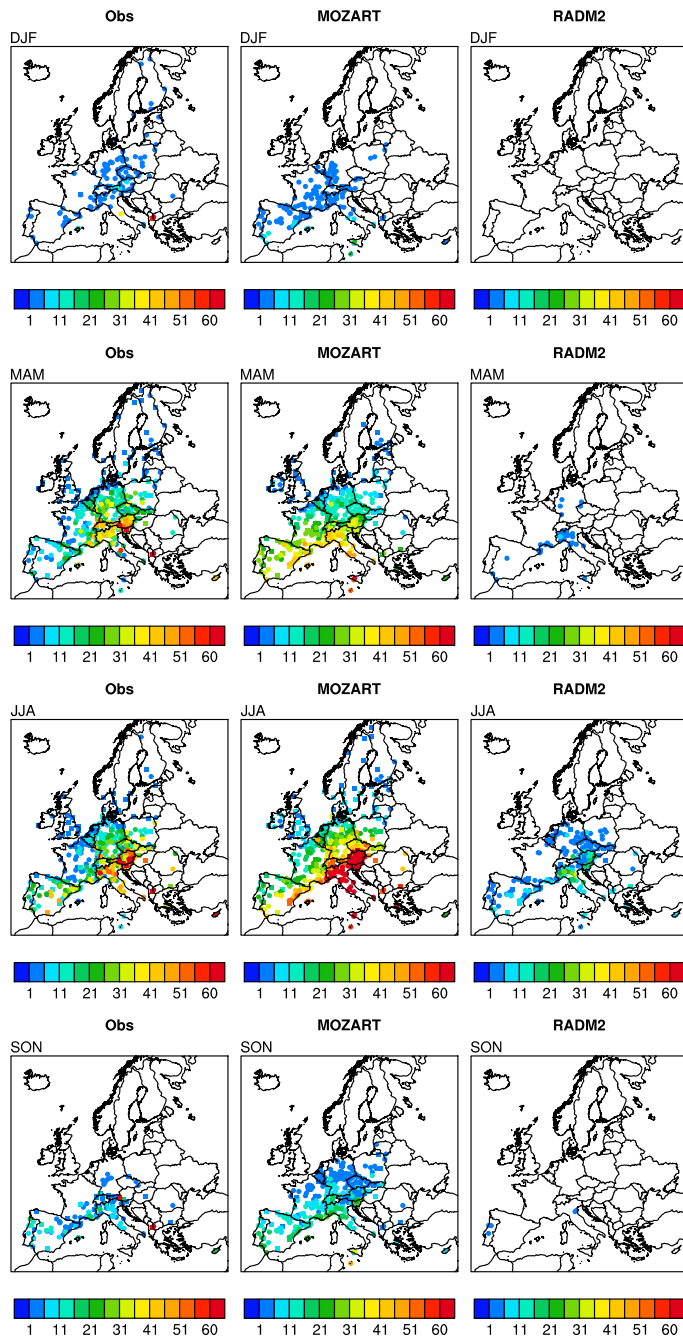
Figure 7. Number of days of exceedances of the EU long-term objective value for MDA8 (120 $\mu\mathrm{g\,m}^{-3}$) at AirBase (circles) and EMEP (squares) station locations. Shown are totals by season for observations and the MOZART and RADM2 simulations. For simplicity of viewing the data, stations with no exceedances are not plotted.
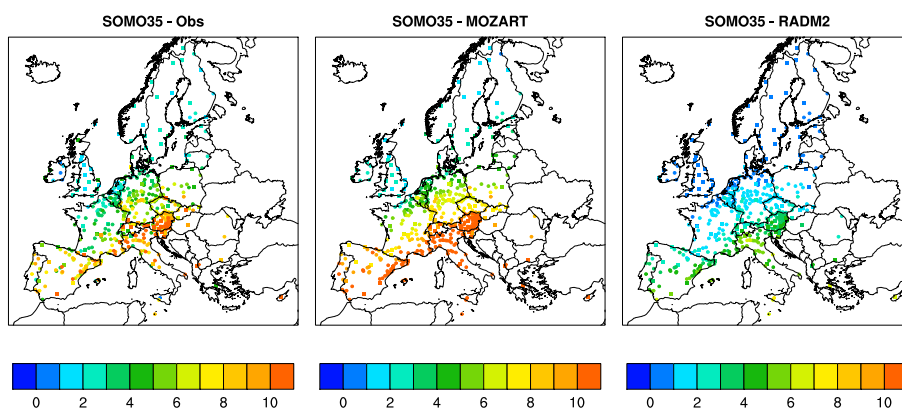
Figure 8. Yearly values of SOMO35 in $\mathrm{mg\,m}^{-3} \cdot \mathrm{days}$ calculated from hourly measurements at AirBase (circles) and EMEP (squares) stations, and modeled values for corresponding locations.
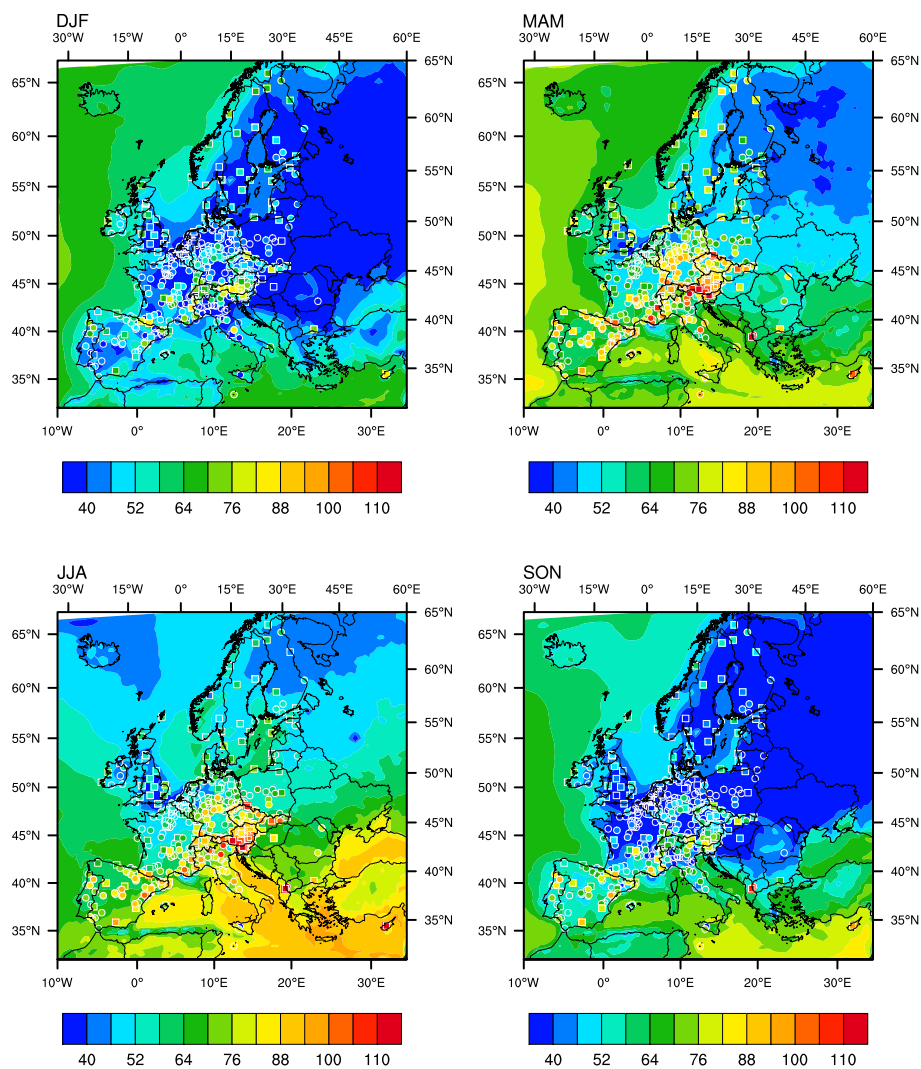
Figure 9. Seasonal average values of surface O_3 in µg m^{-3}. Contours are model output from the RADM2 simulation. Filled dots represent hourly measurements at AirBase rural background stations, filled squares represent measurements at EMEP stations.
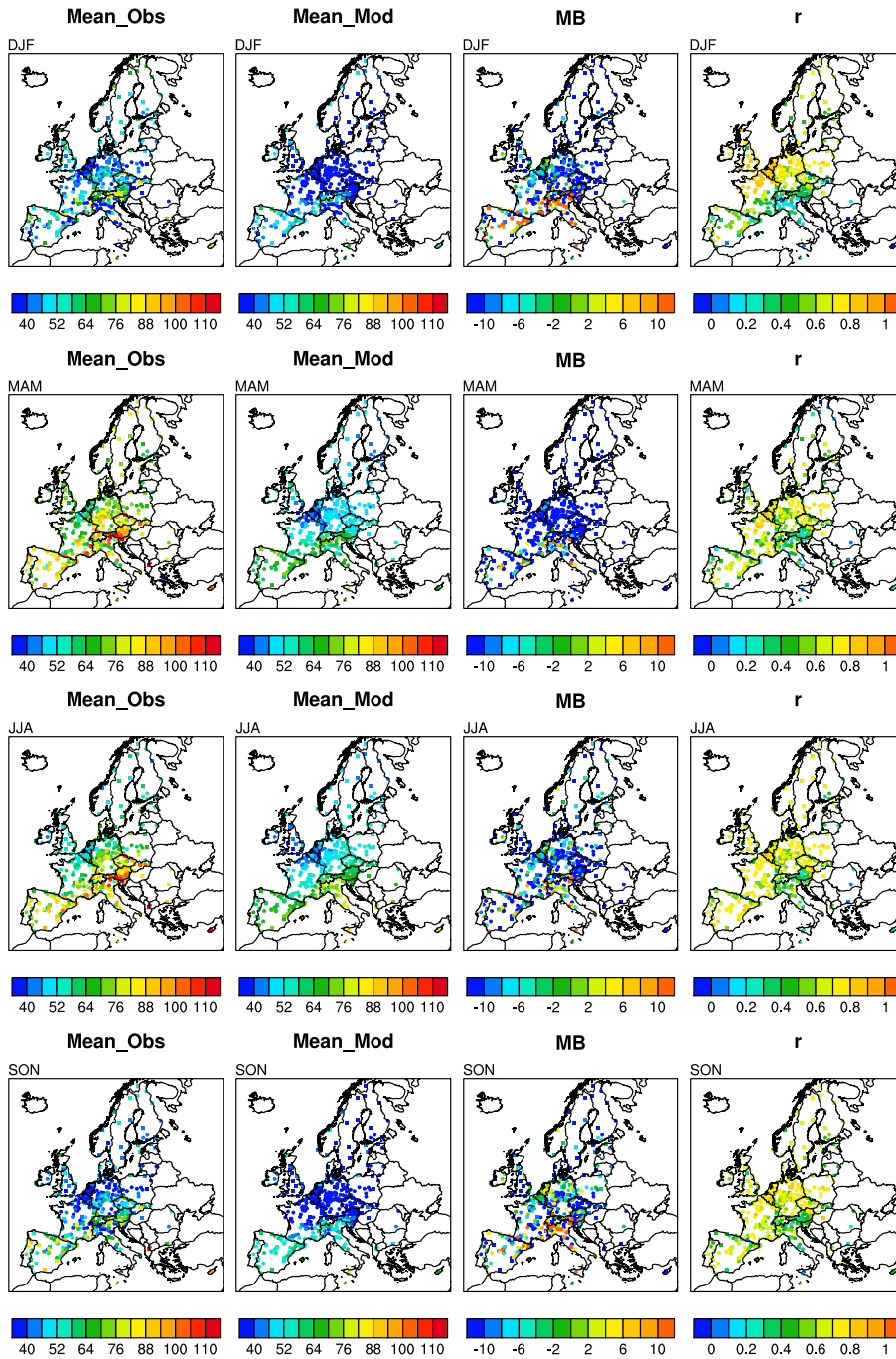
Figure 10. Seasonal average values of surface O_3 in $\mu g\,m^{-3}$ from hourly measurements at AirBase (circles) and EMEP (squares) stations, and modeled values from RADM2 for corresponding locations. The Mean Bias (MB, in $\mu g\,m^{-3}$) and temporal correlation coefficient (r) for hourly values are also shown at the location of station observations.
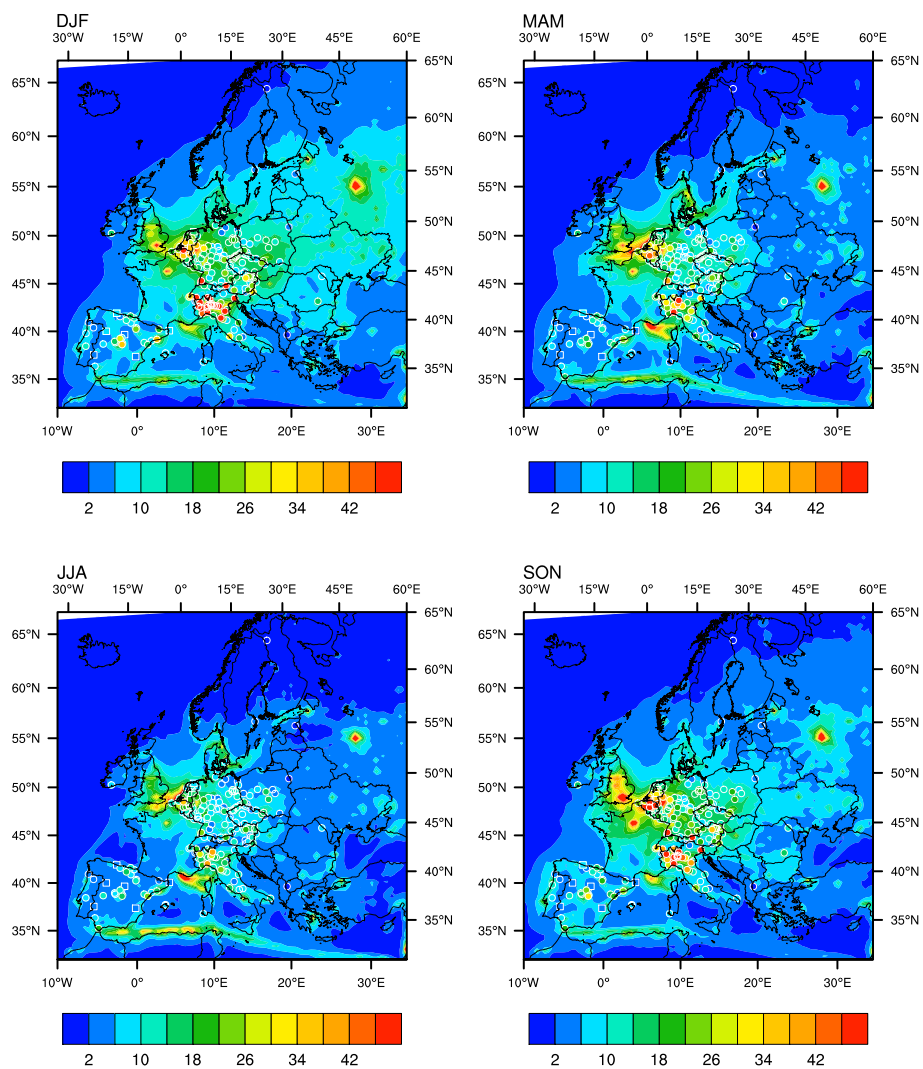
Figure 11. Seasonal average values of surface NO_x in $\mu g\,m^{-3}$. Contours are model output from the MOZART simulation. Filled dots represent hourly measurements at AirBase rural background stations, filled squares represent measurements at EMEP stations.
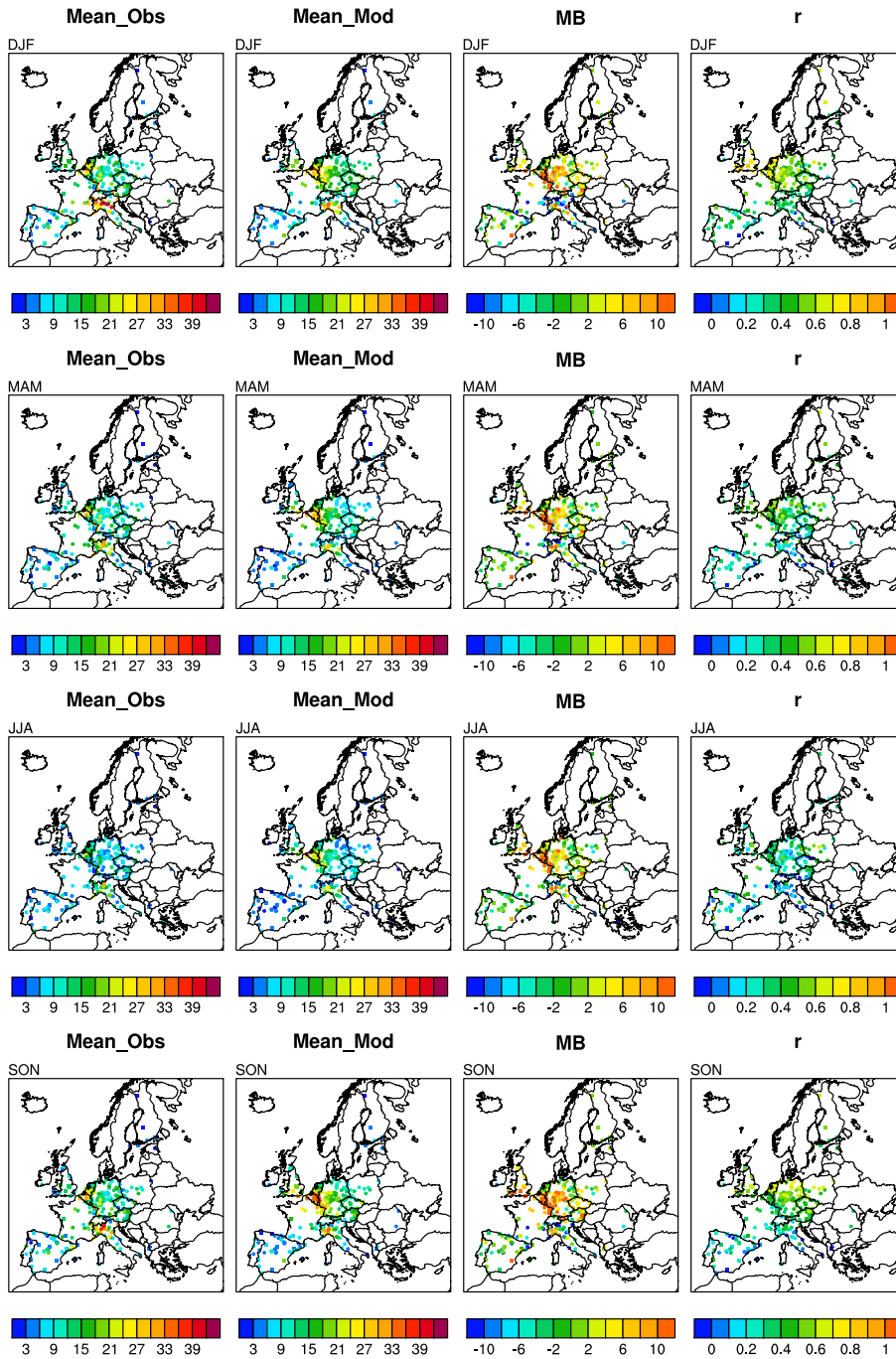
Figure 12. Seasonal average values of surface NO_2 in $\mu g\, m^{-3}$ from hourly measurements at AirBase (circles) and EMEP (squares) stations, and modeled values from MOZART for corresponding locations. The Mean Bias (MB) and temporal correlation coefficient (r) for hourly values are also shown at the location of station observations.
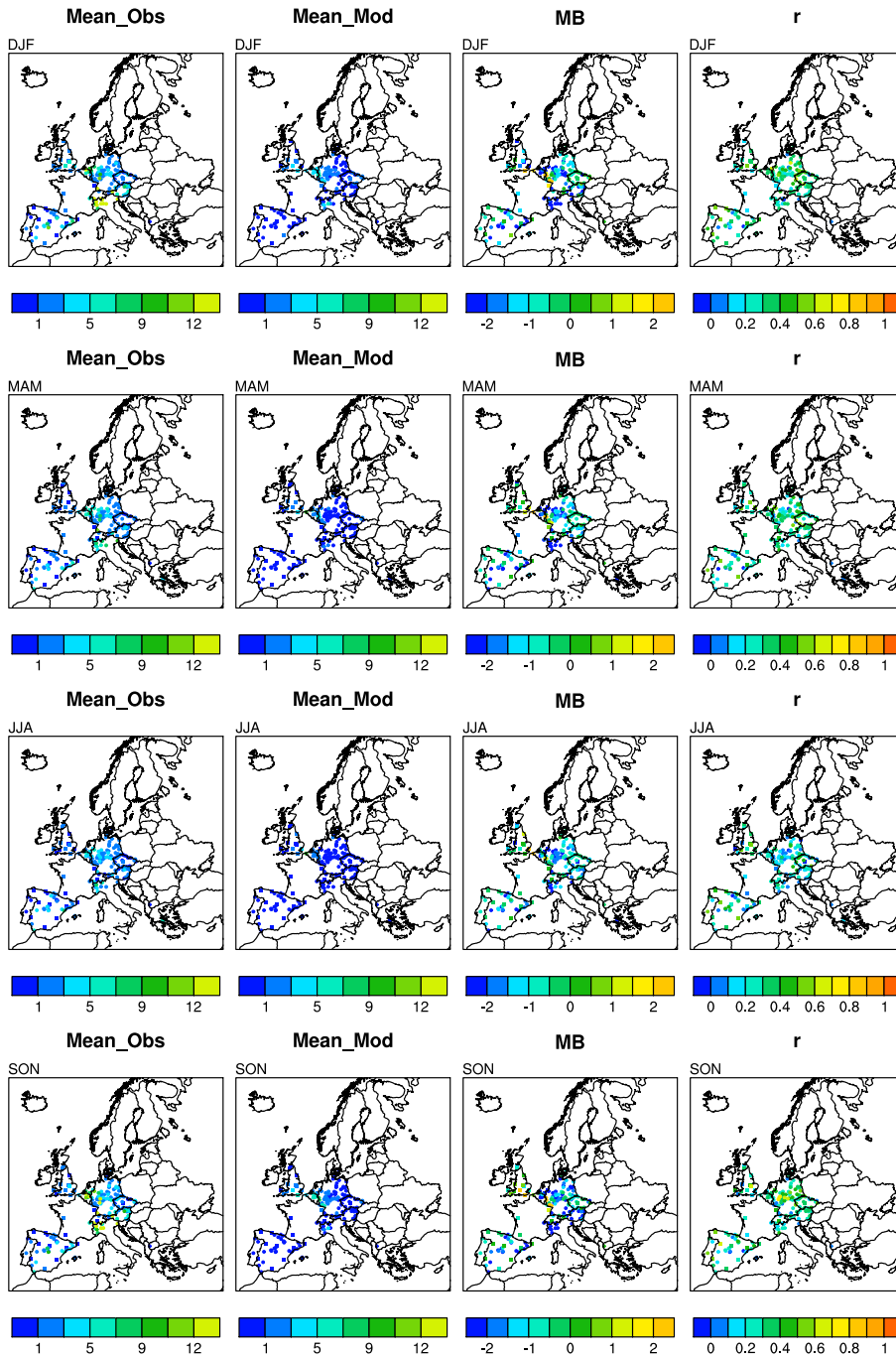
Figure 13. Seasonal average values of surface NO in $\mu g\,m^{-3}$ from hourly measurements at AirBase (circles) and EMEP (squares) stations, and modeled values from MOZART for corresponding locations. The Mean Bias (MB) and temporal correlation coefficient (r) for hourly values are also shown at the location of station observations.
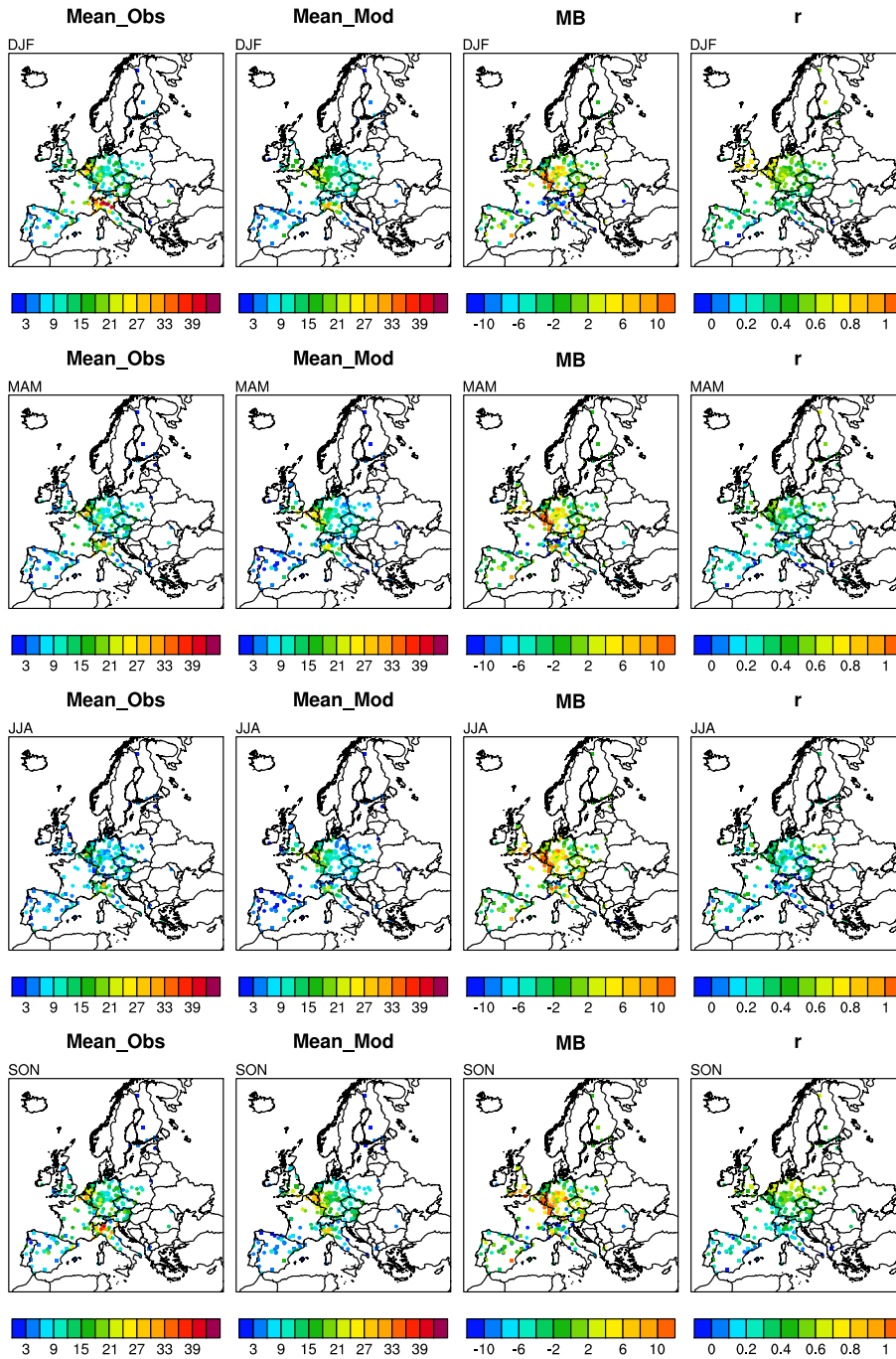
Figure 14. Seasonal average values of surface NO_2 in $\mu g\,m^{-3}$ from hourly measurements at AirBase (circles) and EMEP (squares) stations, and modeled values from RADM2 for corresponding locations. The Mean Bias (MB) and temporal correlation coefficient (r) for hourly values are also shown at the location of station observations.
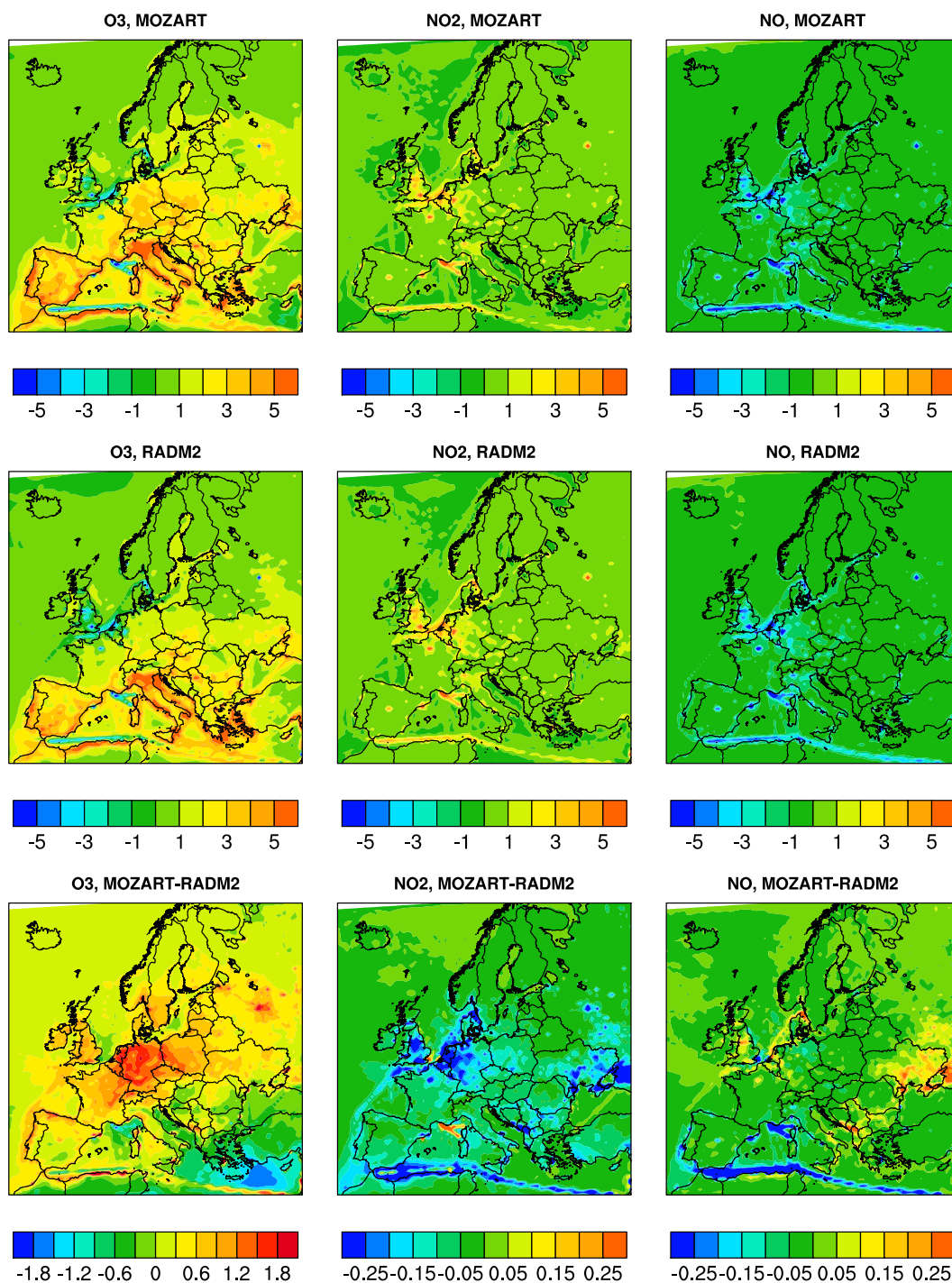
Figure 15. Net midday (11:00 - 14:00 CEST) photochemical production rate in $\mathrm{ppb\,hr^{-1}}$ for O_3, NO_2, and NO shown for MOZART and RADM2 for July 2007. The last row shows the difference in net production rate in $\mathrm{ppb\,hr^{-1}}$ (RADM2 subtracted from MOZART).
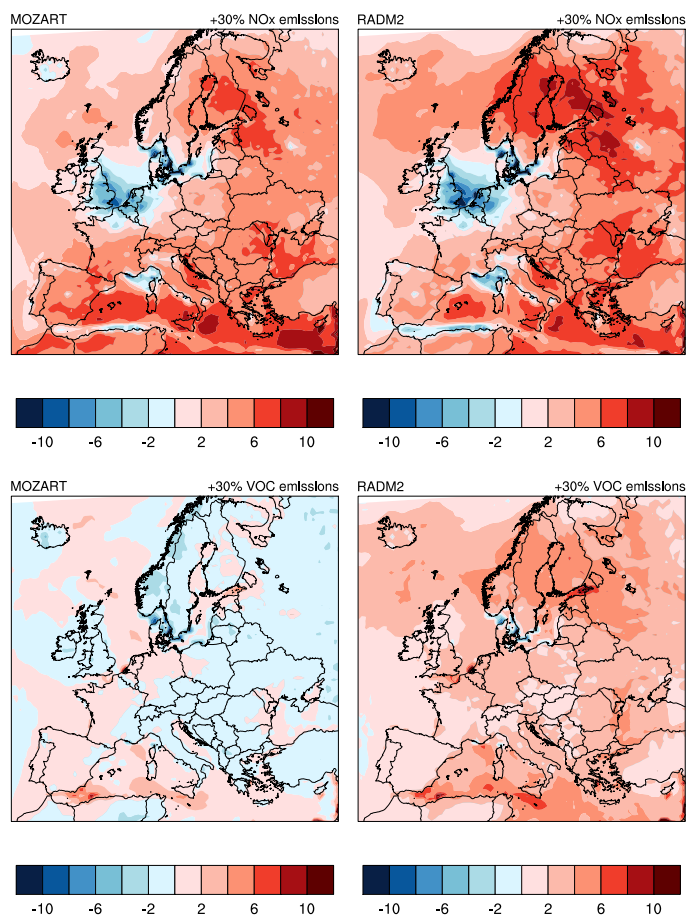
Figure 16. Sensitivity of average O_3 for July 2007 to a 30% increase in emissions of NO_x (upper row) or VOC (lower row), shown for the MOZART and RADM2 chemical mechanisms. Shown here is the percent change in O_3 concentration, i.e., $100 \times ([O3]_{+30\%\mathrm{emissions}} - [O3]_{\mathrm{base}})/[O3]_{\mathrm{base}}$.